CHALMERS

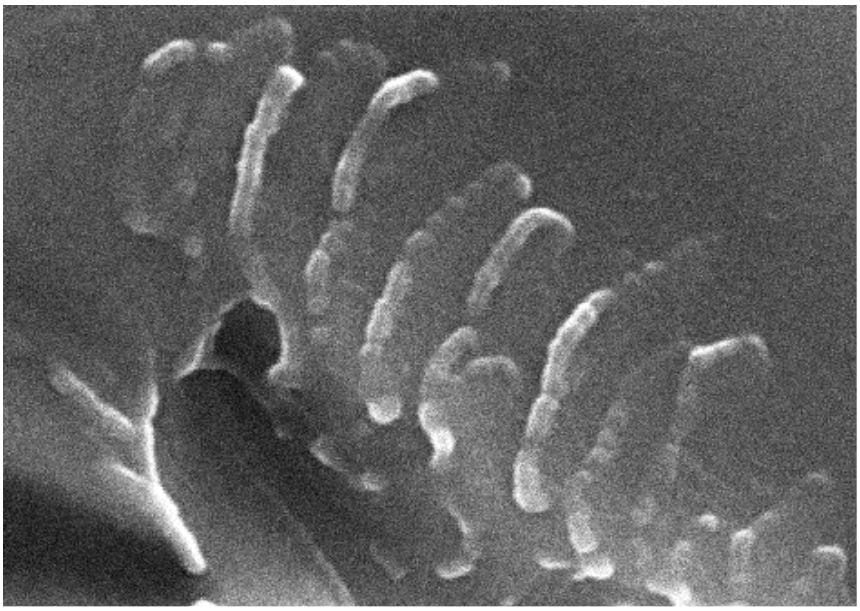

Characterization of nanocomposites for OPL applications

ROBERTO VAN GELDEREN LÓPEZ

Department of Materials and Manufacturing Technology
Surface and Microstructure Engineering
CHALMERS UNIVERSITY OF TECHNOLOGY
Göteborg, Sweden 2013
Thesis 2013

Characterization of nanocomposites for OPL applications

ROBERTO VAN GELDEREN LÓPEZ

Department of Material and Manufacturing Technology
Surface and Microstructure Engineering
CHALMERS UNIVERSITY OF TECHNOLOGY
Göteborg, Sweden 2013

Characterization of nanocomposites for OPL applications

ROBERTO VAN GELDEREN LÓPEZ

Examensarbete / Institutionen för material och tillverkningsteknik,
Chalmers tekniska högskola 2013

Department of Materials and Manufacturing Technology
Surface and Microstructure Engineering Chalmers University of Technology
SE-412 96 Göteborg
Sweden
Telephone: + 46 (0)31-772 1000

Cover:
SEM image of fracture surface of sample P1610.

Characterization of nanocomposites for OPL applications

ROBERTO VAN GELDEREN LÓPEZ
Department of Material and Manufacturing Technology
Surface and Microstructure Engineering
Chalmers University of Technology

ABSTRACT

This project concerns the characterization of nanocomposites of ferrite oxide ($NiFe_2O_4$) and carbon black in poly-metal methacrylate (PMMA) for optical power limiting (OPL) applications. This is due to their non-linear optical properties and behavior at nanosize.

Polymers show an improvement in properties when they are alloyed with nano-fillers. The polymer-based nanocomposites which are used for OPL applications need to be characterized for particle distribution in relation with their optical properties, milling time and particle concentration.

To determine the particle distribution, the fracture surface was analyzed by SEM. Some samples were also dissolved in order to only investigate the particles in the SEM. Sample preparation required for SEM investigation is presented and the difficulties that occur along the process are described.

Keywords: Nanocomposites, Optical Power Limiting, SEM, Mechanical Alloying, Particles.

Contents

Preface

In this study, characterization of polymer nanocomposites was performed. The work has been carried out between April and July 2013 as part of a research project concerning non-linear optical properties of polymer nanocomposites. The project is carried out at the Department of Materials and Manufacturing Technology, Chalmers University of Technology, Sweden in collaboration with F.O.I., the Swedish Defense Research Agency, Sweden.

This part of the project has been carried out by Roberto van Gelderen Lopez as a experimentalist and Professor Uta Klement as supervisor. All tests have been carried out in the laboratory of the Department of Materials and Manufacturing Technology at Chalmers University of Technology. I would like to thank my coordinator, Uta Klement, Raquel De Oro, Yiming Yao and Ruth Ariño for their eternal patients and help along this project.

Göteborg, September 2013

Roberto van Gelderen López.

1 Introduction

Optical Power Limiting (OPL) material are of importance in different fields like computing, protecting sensors from lasers [1], future optical computing [2] and eye protection against high power laser [1]. The main advantage of this kind of materials is its self-activated behavior with high intense lights; it is decreasing the transmittance with an increase in light intensity [1, 3]

The incorporation of nanocrystalline metallic particles in a polymer matrix improves the optical properties of the metallic nanoparticles and the mechanical characteristics of the polymer [4]. Providing materials with good mechanical and optical properties will meet the requirement for OPL application.

2 State of the art

This literature research provides a description of the different factors that affect the optical properties of the nanocomposites, as well as the procedures used for investigating them. Also, the state of the art within the research field is described.

2.1 Effect of the particle parameters on the optical properties

The particle parameters (content, size, distribution, etc.) affect the optical and non-linear optical properties of the nanocomposites [5]. A narrow particle size distribution is required to improve the optical properties [2]. It has been described by Srivastava [4], that it is difficult to reach a homogeneous particle distribution in the polymer. However, a similar surface polarity of matrix and nanoparticles helps in dispersing the particles in the polymer [6].

Different kinds of studies have been carried out to describe the interaction of such nanocomposites with visible light. Transparency and good transmittance in most of the visible spectrum is required for achieving OPL properties. In case the material is intended to act as a protection against green laser light, the transmittance has to be limited at a wavelength of 532 nm [3].

2.1.1 Transparency

Transparency is one of the requirements for OPL material. Light scattering in the composite is responsible for the loss in transparency [2, 6]. It is affected by particle size, the quality of particle dispersion and is inversely affected by particle content. The light scattering is mainly caused by the difference in refractive index between polymer matrix and the particles, which is directly related to density variations [6]. Transparency is also affected by surface roughness. As long as surface roughness is in

the submicron range, it does not influence transparency, but whenever the roughness gets larger transparency decreases. Additionally, inorganic particles can increase the crystallinity of the polymer matrix and decrease the transparency due to inhomogeneous nucleation [6].

2.1.2 Light transmittance

Light transmittance is defined as the percent of incident light that goes through the media, in this case the nanocomposite. The transmittance, as the light scattering, is affected by the difference in refractive index [6]. However, for small particle size (normally < 25 nm) this mismatch is negligible. For bigger particles, the difference must be reduced to avoid scattering [2]. It is also affected by the amount of particles in the nanocomposite, i.e. an increase of the particle content reduces light transmittance through the composite [3].

As mentioned before, for applications as green laser protection, the wavelength must be limited. This limitation is associated with particle size (single particles and agglomerates), size distribution, distribution [6] and the amount of particles in the composite [4]. The particle size and the particle amount act on the absorption shift, while at the same time the particle size distribution influences the strength of the quantum effect for a particular wavelength [2]. A homogeneous particle distribution is required to offer a uniform behavior along the entire composite.

2.1.3 Haze and clarity

The difference between haze and clarity is the angle range in which the light is scattering. A wide angle range means more haze and a narrow angle range means more clarity [7]. The main parameter that acts on haze is the difference in the refractive index between the polymer matrix and the particles. Haze increases with the particle content because of the scattering and reflection of the light. In contrast, clarity is mainly affected by the particle size and the amount of agglomerates present. It is not affected by the difference in refractive index [6].

2.2 Optical power limiting materials

The best optical limiters are those which are transparent for low energy laser and opaque for high energies. In OPL materials, the limiting threshold is a significant parameter. For a better optical limiting response, a low value of the optical limiting threshold is required which decreases with an increase in particle size [8].

Optical power limiting is a result of the non-linear optical response of the nano-materials [8]. For this application different materials have been studied as matrix material and as nanofiller.

2.2.1 Matrix

For OPL applications, a high transparency and good optical properties are important for the matrix material, since transparency loss will occur when the nanofillers are included. Also of interest are good mechanical performance and low price. Of the different materials offering these properties to more or less extend, glasses, ceramics and polymers have been studied. Ceramic and glass as matrix material can enhance the mechanical, thermal and optical properties of small particles [2]. However, a polymer matrix offers a better behavior when it is compared with inorganic glasses, i.e. it shows a lower weight and a better impact strength [6].

After deciding for a polymeric matrix material, there is still a choice to be made between poly methyl methacrylate (PMMA), polycarbonate (PC), polystyrene (PS) and chitosan based on their transparency and mechanical properties. Analyzing the different polymers and comparing their properties as matrix material, PMMA seems to be best suited.

All of the materials present high transparency [9] as well as good dimensional stability [3, 9] and mechanical properties. The first problem appears with the higher light sensitive of PC and PS; they turn yellow and lose their mechanical properties when being expose to light (UV light for PC) [9]. The PMMA shows better optical properties than PC and PS, as well as a higher tenacity than PS and a lower price than PC [9]. In addition, the PC is hydrophilic in contrast to PMMA which is hydrophobic, resulting in larger particle agglomeration in the PC [6].

The mentioned polymers are synthetic petroleum based polymers. Hence, they show poor biodegradability and are influenced by the variations in the petroleum market that is showing an incipient price rise [10]. Using chitosan as biopolymer offers some advantages as availability, low price, biodegradability, excellent film forming, etc. It also has the disadvantage of having poor mechanical properties and low thermal stability, rigidity, etc, limiting its use for many applications [10]. However, chitosan presents interesting properties when it is alloyed with nanoparticles, i.e. a low weight percent of alloying additions have a high impact on mechanical properties, barrier properties and higher transparency. This improvement depends on the nature and surface functionality of the nanofillers [10]. The biggest problem with chitosan is the difficulty to produce transparent nanocomposites, requiring its dissolution in other materials e.g. acetic acid [3].

Nowadays, PMMA seems to be the best choice as matrix material for OPL applications. Nevertheless, chitosan can be the future polymer for this kind of applications.

2.2.2 Fillers

The most important fillers used in this kind of application are the nickel iron ferrite particles, carbon black and fullerenes (C_{60}). Investigations have also been performed with noble metals, alumina, and silica. However, only the results from using nickel iron ferrite and the carbon black as fillers will be discussed here.

2.2.2.1 Nickel iron ferrites

The spinel ferrites showed good results when they were analyzed for OPL properties in microemulsions and nanoparticle suspensions [3]. They show high corrosion resistance, high electrical resistivity and exceptional magnetic properties at high frequency. The nonlinear properties can be controlled by a magnetic fields [8]. Thomas et al. [8] have stated that there is a relation between the particle size and physical and chemical properties in the nano range. Due to the broad range of possible applications, many investigations concern also the magnetic behavior of $NiFe_2O_4$ particles.

As can be seen in Fig.1, the $NiFe_2O_4$ is an inverse spinel where the divalent cation (Ni^{+2}) and some of the trivalent cations (Fe^{+3}) will take the octahedral holes while the other trivalent cation will occupy the tetrahedral holes [11]. The high-energy milled $NiFe_2O_4$ has a nanostructure with a low concentration of iron cations on tetrahedral sites. Spin canting and the mechanically induced changes in cation distribution are responsible for its structural and magnetic disorder [12]. The difference in magnetic behavior of bulk and nanosized nickel ferrite is related to the structure, i.e. nanoparticles present core-shell morphology with collinear aligned core spins and a shell which shows a spin glass structure [13, 14]. The structure flexibility of spinel ferrites allows a broad range of physical behaviors [12].

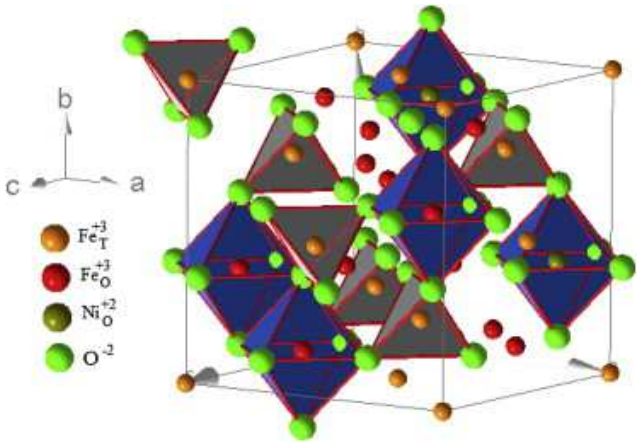

Figure 1: Inverse structure NiFe2O4[15] Printed with the permission of the authors.

The nanocomposite performance is correlated with how well the nanoparticles are dispersed in the matrix and the nature of the non-magnetic polymer [13]. The magnetic behavior of the nanostructured particles is related to the manufacturing process of the powder [14, 16], the particle interactions and the particle size [16, 17]. The particle size is related with the magnetic behavior through the critical diameter, D_c. If the particle size is larger than the critical diameter, the particles present multi-domain structure (areas with uniform magnetization are divided by domain walls); in case the particle size is below the critical diameter, a single domain structure is established (all spins are oriented in the same direction in the particle).

There are differences between bulk and nanostructured ferrites that affect the behavior of the material. The bulk ferrite shows ferrimagnetic behavior, while superparamagnetic behavior is found in milled ferrite [12]. When the powder is annealed over 600 K, recrystallization sets in and the material loses the special properties that the nanostructure offers [12].

The milled nickel ferrites show different behavior below and above the blocking temperature (T_B), which is defined by different factors like the particle´s size, the effective anisotropy constant, the magnetic field applied and the experimental measuring time, increasing T_B for a shorter measuring time [17]. Below the blocking temperature, the magnetic moments are blocked, presenting a remanent magnetization and coercivity. However, above T_B, the nanoparticles become single magnetic domains when being under the critical diameter which normally is 10-20 nm [17]. They are then free to move and align with the magnetic field present, exhibiting superparamagnetic characteristics like absence of hysteresis, nearly zero coercivity and remanence [13]. It is also important to mention that superparamagnetic nanoparticles do not tend to form agglomerates at room temperature [17]. Even at high magnetic fields, the particles do not present saturation, which indicates a hard surface pinning and a spin glass effect [13] that has been associated with a magnetization reduction [17].

Thomas et al. [8] have studied different ferrites for OPL properties using nanosecond laser pulses at 532 nm and established that the best OPL properties are found for the $ZnFe_2O_4$ instead of $NiFe_2O_4$ due to a better nonlinear optical response with a lower optical limiting threshold for the same particle size.

2.2.2.2 Carbon black

Carbon black is the result of an incomplete combustion or thermal decomposition of gaseous or liquid hydrocarbons under specified conditions, and is different from black carbon or soot [18]. For OPL applications, the carbon black is mainly studied in suspension (CBS) or placed on a microscope slide (CBG).

The mechanism governing the limiting behavior in the carbon black suspensions (CBS) and carbon black particles deposited on glass (CBG) is nonlinear scattering [19-21]. This nonlinearity is explained by the quick heating of the particles that leads to vaporization and ionization of the particles, forming a microplasma that rapidly expands [19, 20]. But also the internal structure of the particles influences the optical behavior of the material [22].

The limiting effect that the carbon black offers changes when the laser is focused on the same position of the sample, since the particles are ionized and vaporized, after irradiation. Hence, they are not effective any more [19]. It is important to take into account that this is valid for laser firing times of nano- and microseconds.

2.3 Mechanical alloying

The milling process is connected with the reduction of the particle size and distribution of the particles in the polymer matrix. This process is of highly non-equilibrium nature, providing the possibility to improve and/or modify chemical and physical properties [12].

During milling, fracture and cold welding of the particles can be anticipated, leading to a crystallite size reduction [13]. The glass temperature should not be reached to keep a good dispersion of the particles [1] and agglomeration must be minimized

because it might act as crack initiator in the composite due to stress concentrations that are created [23]. Different milling processes can be used, e.g. high-energy ball milling at normal or cryogenic temperature and pan milling.

2.3.1 Pan milling

A special pan milling technique used to obtain ultrafine composite powders has been developed and described by Xu et al. [24]. Using this technique for studying composites of polypropylene (PP) and iron, a high size reduction (97,8% after 30 milling cycles) and a good particle distribution was reached in the matrix after the pressing process. A better size reduction was achieved when a mix of particles and polymer was milled instead of only polymer [25].

In this process, a higher amount of coarse particles are present due to pulverization of large particles and agglomeration of the smaller ones. During the process, an equilibrium state of both pulverization and agglomeration can be reached. The agglomeration causes a delay in the counter-grinding process. However, Canhui et al [25], stated that after the 8^{th} milling cycle a large size reduction takes place, also oxidation of the iron particle surfaces occurs, caused by the presence of air during milling.

2.3.2 High energy ball milling

2.3.2.1 Normal temperature

For high-energy ball milling, a better homogeneity of the product is achieved when increasing the milling time [1]. Also, a decrease of PMMA molecular weight [6], a smaller particle size as well as an increase of the mechanical properties and thermal stability of the polymer is established [3]. When nickel ferrite powder is processed with this method, its magnetization decreases due to strains introduced in the particle surface. This stress increases the irregularities of the magnetic moments on the surface, leading to a further increase of anisotropy in the particle´s shell [16]. With respect to the particle dispersion, a better result can be reached when the polymer and the particles were milled together and the temperature does not reach the glass transition temperature of the polymer [3].

However, for small particle size (5-8nm) the size reduction is negligible after milling [13]. Normal temperature milling has higher impact on the molecular characteristics of the polymer and reaches an almost mono-disperse molecular weight distribution [26].

2.3.2.2 Cryogenic temperature

Cryogenic milling has been studied for different kinds of materials, from spices to metals and polymers, using low-temperature gases [27]. Milling at very low

temperature causes important changes in polymeric materials such as a decrease of the molecular weight in PMMA and PET [28]. Also, a reduction in the required energy, an increase in production rates, and lower damage in the milling equipment are achieved [27].

Increasing the milling time, the particles show a better dispersion in the polymer and a higher molecular interaction [28], an increase in the porosity but no significant impact on the tensile strength of the polymer is achieved [29].

2.4 Coating for non-conductive materials

When a conductive coating is required for performing SEM investigations, different materials can be used. The most common coatings are carbon, gold, silver, platinum, palladium, and chromium [30]. A brief comparison between them is given below but focus will be on gold and carbon coatings.

The heavier elements like gold and silver offer a better image quality due to a high secondary electron production. Still, the coating particles tend to migrate and coalesce, decreasing the macroscopic conductivity. There is also a risk that some details of the surface are lost [30].

For high resolution images, elements with small particle size are necessary. For this case, platinum, chromium and osmium are the best options. However, for high resolution SEM, platinum and chromium have still a measurable grain size but osmium shows better results since only a 1 nm thick layer is needed for achieving sufficient conductivity [30].

When applying a gold coating, the plasma treatment and the gold layer have different effects on the polymer. Kotál et al. [31] describe the effect on polyethylene terephalate (PET) where the plasma treatment increases the surface oxygen concentration and the surface wettability. However, both decrease with time. The decrease of the surface wettability is due to the contact with the atmosphere, resulting in a higher reduction in samples treated for more than 30 seconds [31].

The gold sputtering increases the roughness of the polymer surface keeping the topography almost intact; increasing the microhardness and decreasing the elastic modulus in the plasma treated samples. These factors may be related with the cross-linking that the plasma discharge causes, increasing the difficulty for the metal particles to diffuse along the polymer. A good adhesion between the coating metal and the polymer depends of the metal-polymer interface [31].

A carbon coating is of interest for microanalysis due to its transparency and electrical conductivity [30, 32]. The visible light transmittance is quite low in films made in pure argon but it increases substantially when hydrogen is added during the sputtering (between 1 and lower than 10 percent) [32]. The visible light transmittance is better at lower sputtering power. However, the difference when using higher sputtering power is so small that it is preferred because of the better mechanical properties that can be achieved [32]. The higher impulse voltage decreases the roughness across the surface because of a higher ionization and the carbon ions coat the surface with more energy but also increase the internal stress [33].

2.5 SEM for non-conductive materials

There are different ways to study polymers in SEM: low voltage (with and without coating), high voltage (degrades the sample) and variable pressure [34]. The SEM studies on composites were performed on fracture surfaces [23, 34], where the particle distribution is easier to be observed and other information like loading history, extension of process zones, etc. [34] can be deduced.

For non-conductive materials, a good conductivity over the surface is required to avoid image charge build-up [23, 34]. Especially the secondary electron imaging mode has a tendency to charge the sample [23]. An increase of the beam voltage also enhances the charging effects. To compensate for this enhancement, a higher chamber pressures is needed which in turn increases the noise level and leads to a decrease in resolution. On the other hand, a lower beam voltage offers a worse description of the surface relief [34]. Texture information and resolution are related with the SEM parameters; resolution is related in a non-linear way with the parameters [34].

Investigations carried out by Hein et al. [34] on coated and un-coated samples by use of AFM show an insignificant variation of the topography of the samples for coating thicknesses lower than 25 nm but also leads to an increase of the size of objects at the surface. However, this is valid for magnifications lower than 7000x since the coating layer cannot be observe. For high magnification the coating thickness must be known. Nevertheless, it has been found that a 6 nm thick coating layer is enough for most of the polymer samples [34].

3 Materials and procedure

3.1 Material

In this study, the materials being investigated are carbon black, nickel iron ferrite and PMMA. However, only the producer of the nickel iron ferrite and of one of the PMMA materials is known. All the nickel iron ferrite nanoparticles were provided by *NanoAmor Nanostructured & Amorphous Materials, Inc.* (Appendix B).There are two different PMMA materials used in the composite samples. One PMMA, provided by *Lucite International Co.* (Appendix A) is used in the following samples: G0000, P1600, P1605, P1610 and G1210; the other PMMA was provided by an unknown company. The specific data for each material is provided in the appendix.

The samples without name (Table 1) show some contamination from the container in which the milling was performed. Rust was present in the container contaminating the sample and affecting the transmittance of the nanocomposites [3]. In Table 1, the studied samples are provided.

Table 1: Filler content and milling time of the samples investigated in this study
(* Values taken from T. Faury´s Master thesis [3])

	Percent	Milling time	UV-vis spectroscopic measurement (transmittance at 532 nm)*	Samples names
Carbon black	0,01	12000	10,75%	-
	0,005		23,29%	-
$NiFe_2O_4$	0,1	4000	11,19%	-
		12000	-	G1210
		16000	-	P1610
	0,05	4000	29,12%	-
		16000	-	P1605
	0,01	4000	62,46%	-
		6000	66.67%	-
Not alloy	0	0	-	G0000
		16000	-	P1600

3.2 Procedure for performed studies

The following procedure was used for the investigation of all samples. Different factors required changes in the preparation steps without affecting the samples. These changes are due to the sensibility of some preparation parameters, especially in the carbon sputtering.

Often, no particles were seen in the SEM images. Hence, some samples were dissolved in acetone in order to study a thinner layer of composite with higher particle content. After dissolving the sample and when enough acetone has evaporated, some drops of the remaining solution were deposited on a microscope slide until all the acetone evaporated. First, the obtained samples were studied in the optical microscope. Afterwards, the samples were investigated in the SEM after applying a thick coating layer (15 sec sputtering time). An accelerating voltage of 10 kV was applied together with a working distance of 4 mm. Medium/big spot size was used to reach good image quality at 20 000x magnification.

The steps used for preparing the samples are given in Table 2.

Table 2: Procedure for SEM studies

	Important parameters	Observations
Sample cutting	- Diamond saw. - Water as cooling liquid.	- Cover the sample to avoid surface scratches. - Avoid high pressure on the holder.
Sample fracture	- At least 2 minutes in liquid nitrogen.	- Use small amount of liquid nitrogen to avoid excess of evaporation.
Cleaning	- Isopropanol	- Submerge sample in Isopropanol and apply pressured air.
Carbon coating	- 8 seconds of sputtering. - ≈ 1 cm between the graphite and the sample.	- Contact surface between graphite sticks has to be as small as possible. - A conductive wire has to be painted between the fracture surface and the holder. - Use a white paper to check the coating thickness. - Sputter coater S150B with carbon evaporation S150 from company Edwards.
Scanning Electron Microscope (DSM 940A from the company Zeiss)	1- Voltage: 5kV until 5000x then 10 kV. Working distance: 7-8mm Medium spot size. 2- Voltage: ≈ 2 kV. Working distance: 2-3 mm. Small spot size.	1- When the voltage is increased a better definition is reached but charging highly increases. - At 10 kV, better image quality with bigger spot size is achieved. 2- Not useful for high magnification (< 5000x) because of really low image quality but for lower magnifications (≥5000x) good image quality is achieved at any spot size. - For low voltage a smaller spot size provides a better image

4 Results and Discussion

From this investigation, different information about the nanocomposites and their characterization in the SEM was achieved.

The results were influenced by the sample preparation, i.e. how long the sample was submerged in liquid nitrogen before it was fractured. When a short time was chosen, the images observed in the SEM show white circles surrounding fragments of polymer (see Fig. 2). When the samples were treated in the liquid nitrogen for longer times the white circles disappear and a less polymer fragments was seen on the fracture surface. Additional SEM images of sample P1610 after being treated shorter and longer times the liquid nitrogen are provided in the appendix.

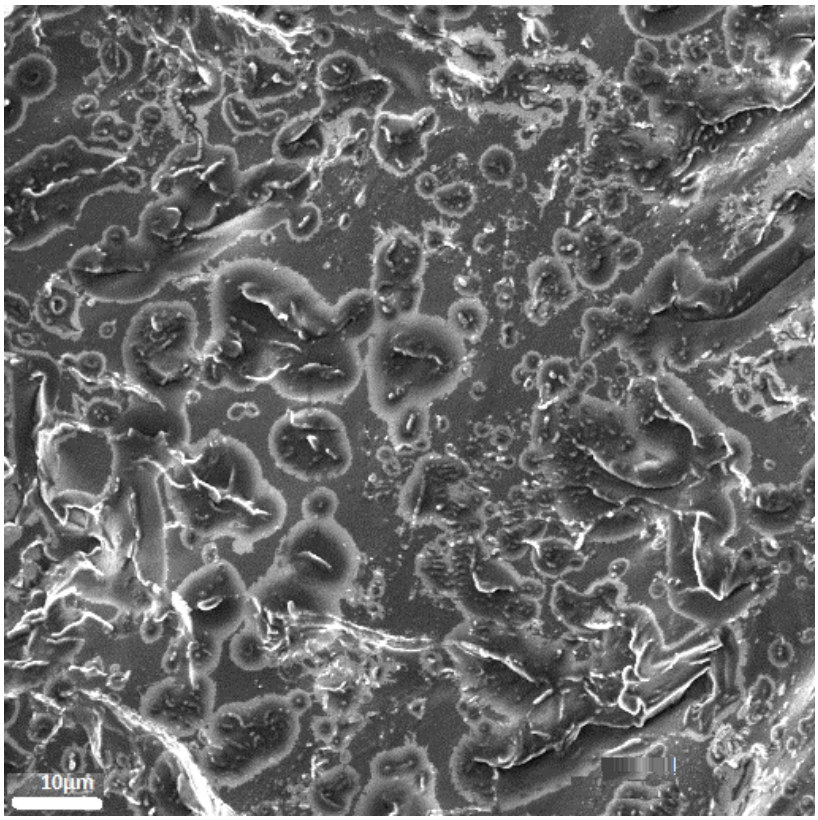

Figure 2: SEM image of sample P1610 (Beam voltage: 5kV; working distance: 12mm).

After a suitable procedure for the fracture of samples with liquid nitrogen was established, the samples were compared with respect to milling parameters. All samples made by the same milling process, i.e. process A in Table 3, showed the same characteristic (Fig. 3) which was very different from the other samples (process B in Table 3). It is assumed that magnetic particles and/or agglomerates line up during the milling (magnetic attraction) and the particle chains remain in the sample during the pressing process. It needs to be mentioned that what is seen in Fig. 3 are particles/agglomerates covered by polymer. However, due to the low amount of particles, the chains of particles are not observed often.

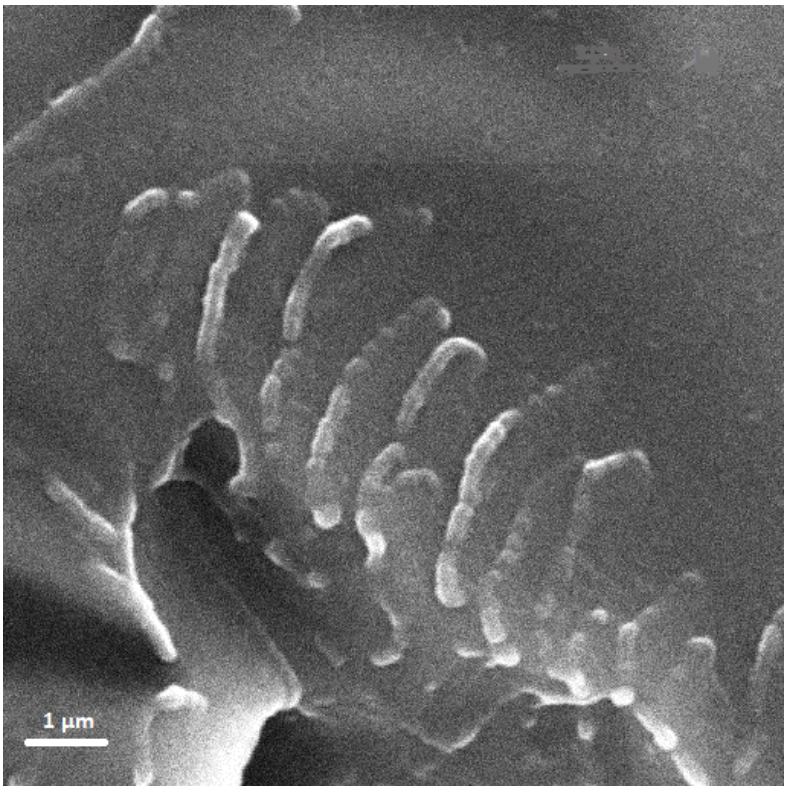

Figure 3: SEM image of fracture surface of sample P1610.

Samples P1610, P1605, P1600, G1210 and G0000 can be compared. All of them were produce by the same process, however milling time, particle content and initial material (granule or powder) was changed. There is the possibility that the features seen in Fig. 3 appear during breaking of the sample after cooling in liquid nitrogen. However, the fact that the chains are seen in the samples with fillers made by process A indicates that the milling process alter the magnetic behavior of the nanoparticles in a similar way as described by Nathani et al. [16] and Šepelák et al. [14].

Table 3: Differences between the sample preparation route A and B

	Samples with pattern (A)	Samples without pattern (B)
Mechanical alloying	- Alumina containers with 2 alumina balls. - Period of 4000 s of milling without stop. - No cooling process after each milling period.	- Container with 3 steel balls. - The milling stops every 5 min to cool down the container with nitrogen.

The low thermal conductivity of the alumina container and the long milling time (12 000 s and 16 000 s in periods of 4 000 s) without cooling down may have increased the temperature of the powder inside the container. The temperature of different samples was measure by Thanon et al. [1] and it never exceeds 45 °C but the

moment when the samples were measure is not specified so the real temperature during processing is unknown.

Knowing that the powder inside the container does not reach the recrystallization temperature of the $NiFe_2O_4$ (≈600 K) [12], the change in magnetic behavior has to be the result of particle size and particle interaction [16, 17]. The initial particle diameter was 20-30 nm. Milling without cooling of the powder reduces the cold work in both the particles and the polymer. This leads to softening of the polymer as result of the increasing temperature and loss of the efficiency of the process [1]. Thus, particle size is reduced less and the single-domain structure is not achieved. Since the superparamagnetic behavior is not reached, the tendency for particles agglomeration is increased [17]. The magnetic behavior is also affected by milling time since it increases the molecular interaction [28]. These factors could alter the magnetic behavior of the nanoparticles allowing the chains to occur that are seen in Fig 3. Therefore, when the samples without fillers (P1600 and G000) were analyzed, no chains were observed but the samples show the same round fragments seen in the samples with fillers ($NiFe_2O_4$ and carbon black). Those fragments (Fig. 4) were first thought to be particles but were identified as polymer by their size, quantity and presence in the samples without fillers. Fragments of different size were seen in all samples at high magnification.

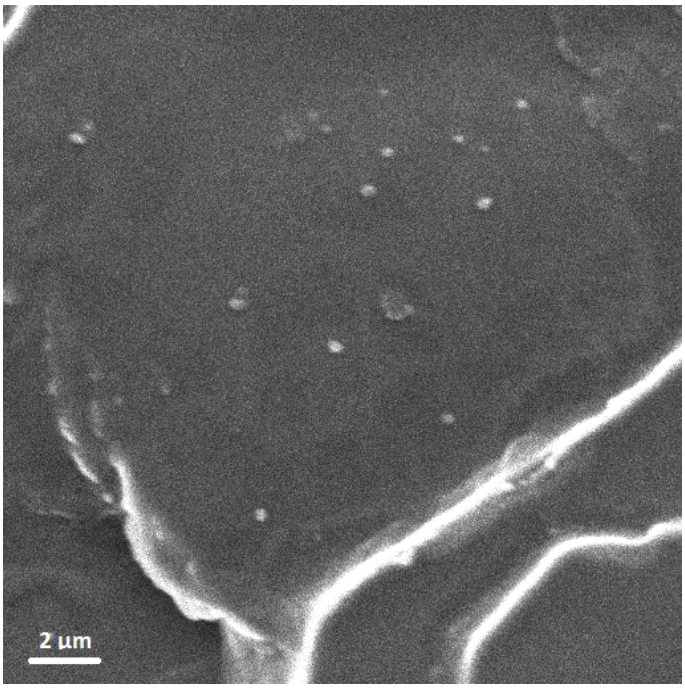

Figure 4: SEM image of fracture surface of sample P1600 showing polymer fragments.

All samples made with help of process B have low milling times and low particle content. The fracture surface after cooling with liquid nitrogen is more irregular and brittle than the other fracture surfaces of samples made by process A with longer milling time and higher particle contents. Fig. 5 shows a low magnification (200x) SEM image of the sample PMMA + 0,01% $NiFe_2O_4$ 4000s.

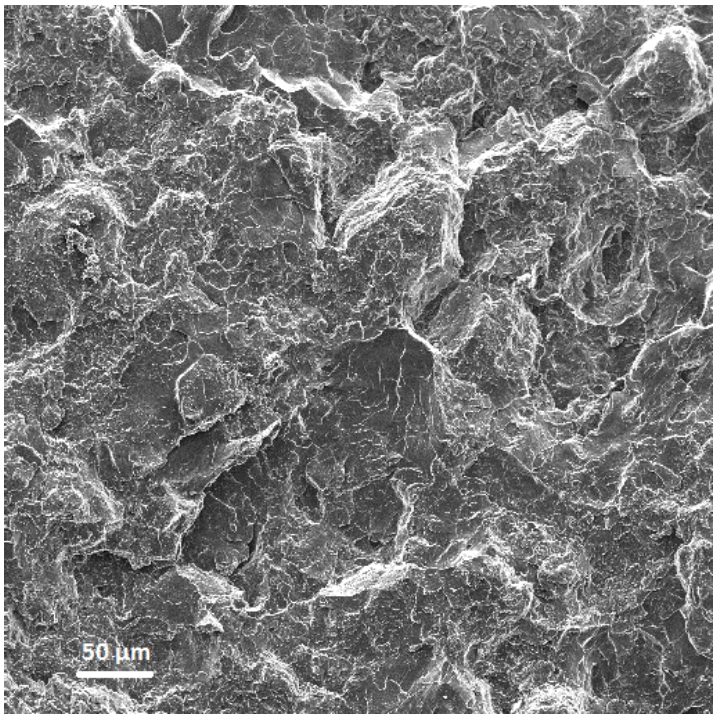

Figure 5: SEM image of the fracture surface of sample PMMA + 0,01% $NiFe_2O_4$ 4000 s

When a higher magnification is used, the same round fragments can be seen. Figure 6 shows them at 5000x magnification. Fragments of different size can be seen and the smallest ones can be easily be confused with particles.

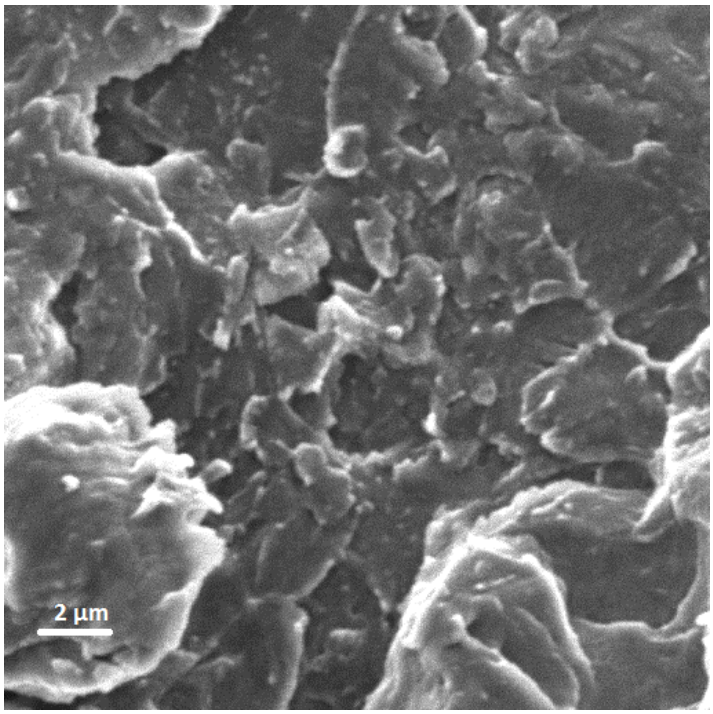

Figure 6: SEM image of the fracture surface of sample PMMA + 0,01% NiFe2O4 4000s.

In connection with the literature research, some suggestions about a better process to produce this kind of nanocomposites can be made:

In order to produce a good OPL nanocomposite for protection against green laser light, the following properties must be provided: high transparency, clarity and low haze, light transmittance in the visible spectrum but limited transmittance at certain wavelengths, e.g. above 532 nm. Also, good mechanical properties, low price and thermal stability are sought since the material has to have enough strength to avoid fracture and good thermal stability (due to the light dissipation heat is generated in the composite).

How these properties are related with the nanocomposite parameters are shown in Fig. 7. It can be seen that particle size is one of the most important parameters. Its control is required for achieving OPL properties.

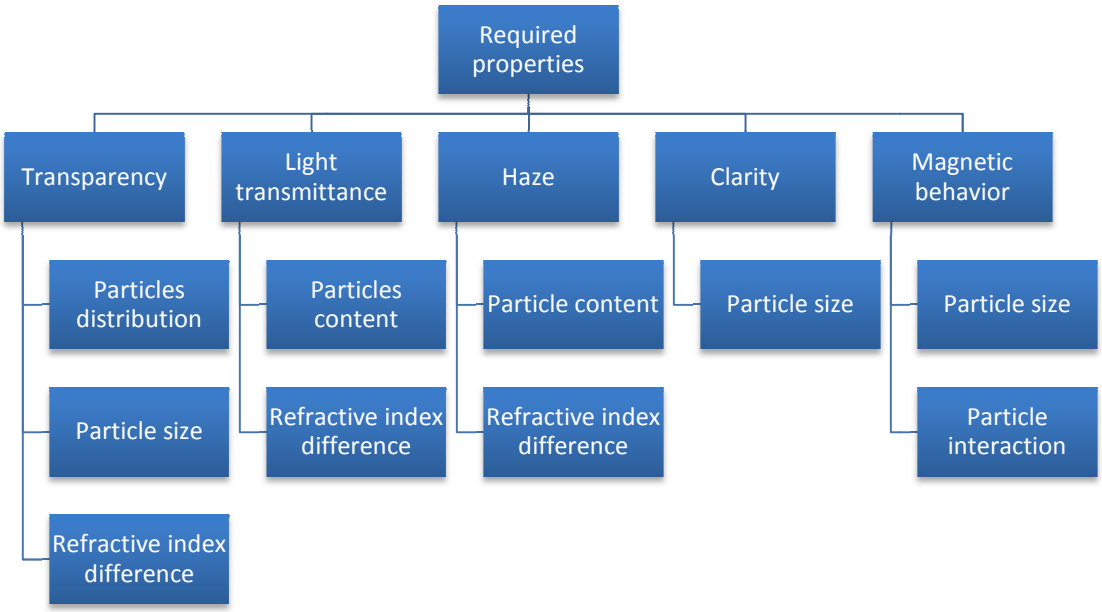

Figure 7: Main properties of an OPL nanocomposite.

Most of these parameters are determined by the mechanical alloying parameters (milling process and milling time) but particle content and refractive index difference can be chosen by the producer. However, the refractive index difference is negligible if the particle size is lower than 25 nm [2]. In Fig. 8, it is shown how the different parameters depend on process parameters.

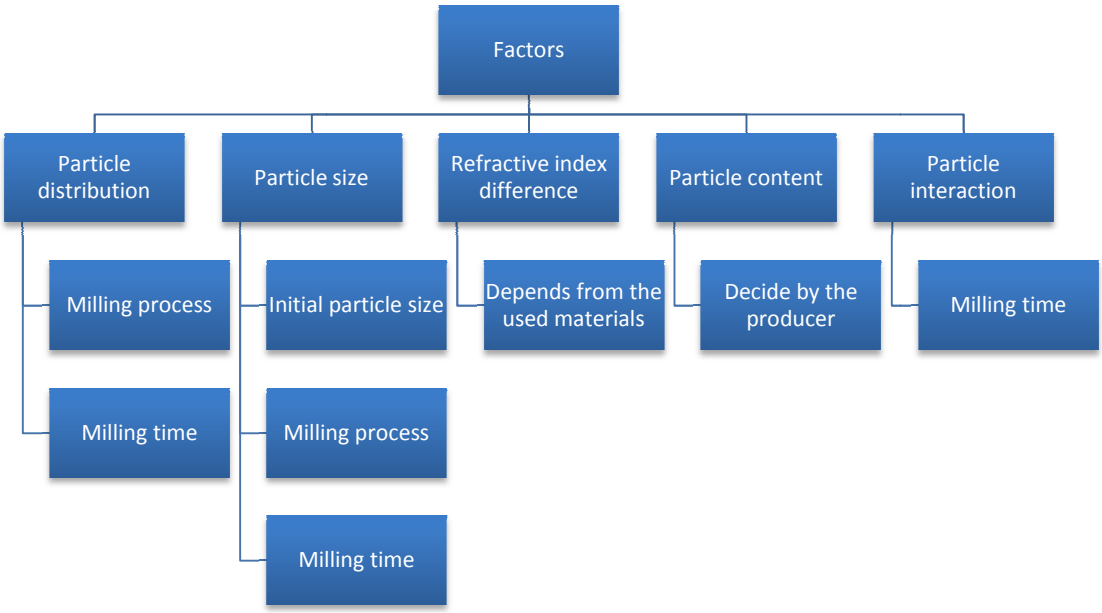

Figure 8: Material parameters and their dependence on process parameters.

From Fig.7 and 8 it is clear that the most important step during the production of this kind of nanocomposite is the mechanical alloying. A careful definition of the milling is required in order to reach the desired properties.

The first decision to be taken concerns the materials and their content in the composite. Once this is decided, the characteristic of the materials before the milling will help to define proper milling parameters in order to reach the sought characteristic after the milling process. From T. Faury´s MSc thesis [3], it can be seen that less than 0,1% of nanofillers is enough to achieve OPL response while some materials require an even lower amount, e.g. carbon black. In the case of carbon black in PMMA , this is due to the large difference in refractive index [6].

To determine the milling parameters, it is important to remember that cold work is the main principle that defines the milling process. For that, a low temperature or a proper cooling is required to avoid a reduction in the milling efficiency [1] and to prevent the softening of the polymer. From the literature research, the cryogenic high energy milling might be the best option. Due to the low temperature, there is no need for additional cooling of the container and a lower milling time is possible. The cryogenic high energy milling increases particle interaction and porosity that might change magnetic behavior [28] and mechanical properties, respectively. In Fig. 9, the effect of increasing milling time is seen. In order to select the milling time, it is important to know the initial size of the particles. A particle size which does not lead to magnetic behavior and removes the refractive index difference (< 25nm) between polymer and particles make easier to obtain a good OPL nanocomposite.

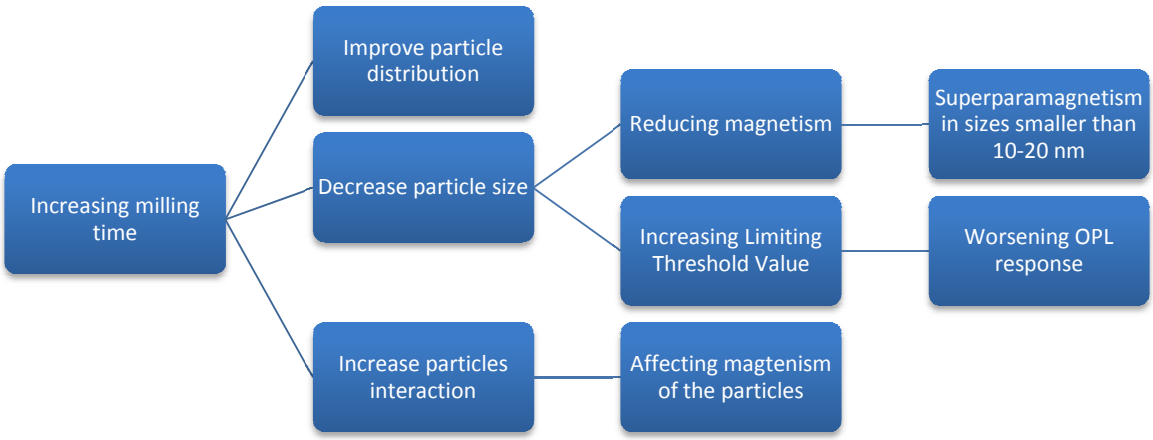

Figure 9: Effect of increasing milling time

From the MSc thesis of T. Faury [3], it can be seen that for the same particle content, a higher milling time increases the light transmittance at 532 nm and for the same milling time, a decrease in the particle content increases light transmittance. Carbon black has profound influence on the OPL properties even at low particle content.

The most important decision at the time when producing the polymer nanocomposites is the dependence of mechanical alloying parameters on content, distribution and size of the particles after milling. A high enough milling time is needed to improve the distribution and to reduce the particle size, avoiding magnetism without major increase of the limiting threshold value and the particle interaction. This milling time depends on the milling process and the particle content.

5 Summary and conclusions

The homogeneity in the distribution of fillers in the polymer matrix is strongly influenced by the milling parameters and the particle size. Therefore, the production of polymer nanocomposite requires special care in the mechanical alloying stage in order to reach the properties needed for a good OPL response. Overheating has to be avoided to maintain milling efficiency.

This project addressed the microscopical examination of nanoparticle distribution by use of a DSM 940A SEM. The results obtained allow providing some hints for future studies:

- The SEM image quality can be improved by using hydrogen (1 to 10 percent) during the carbon coating. Presence of H_2 increases the carbon layer transmittance and thicker coating layers can be applied. The higher carbon content provides a more conductive surface with less charge build-up and offers the possibility of using higher beam voltages for high magnifications.
- During the observation of the samples with the SEM; a low accelerating voltage is better for low magnification images with a small/medium spot size. On the other hand, for the higher magnifications ($\geq$10000x approx.) a high beam voltage with a medium/big spot size offers an improvement in the image quality.

6 Future works

The future steps in this field can be as follows:

- To study the particle distribution in the polymer, a better analysis technique would be Transmission Electron Microscopy (TEM).
- EDS analysis can be performed to state the presence of $NiFe_2O_4$ in the observed chains and to confirm the presence of polymer fragments in samples containing no nanofillers.
- Compare the OPL response for $ZnFe_2O_4$ nanocomposites with $NiFe_2O_4$ nanocomposite to prove the better response stated by Thomas et al. [8].
- Compare the effect of cryogenic high energy milling and the normal temperature high energy milling (with and without cooling down) on the OPL response of nanocomposites.

7 References

1. Thanon, D.J., *Synthesizing materials with non-linear optical properties by mechanical alloying*, in *KTH Industrial Engineering and Management*2009, Royal Institute of Technology: Stockholm. p. 67.

2. Beecroft, L.L. and C.K. Ober, *Nanocomposite materials for optical applications.* Chemistry of Materials, 1997. **9**(6): p. 1302-1317.

3. Faury, T., *Synthesis of new solid state optical power limiting nanocomposites by mechanical alloying.* 2006-2007: p. 32.

4. S. Srivastava, M.H.a.J.K.B., *Optical properties of polymer nanocomposites.* 2008. **31**: p. 213-217.

5. Porel, S., et al., *Optical power limiting in the femtosecond regime by silver nanoparticle-embedded polymer film.* Journal of Applied Physics, 2007. **102**(3).

6. Zhou, R.J. and T. Burkhart, *Optical Properties of Particle-Filled Polycarbonate, Polystyrene, and Poly(methyl methacrylate) Composites.* Journal of Applied Polymer Science, 2010. **115**(3): p. 1866-1872.

7. BYK-Gardner, GmbH. *Transparency*. Website [cited 2013 04/09/2013]. http://www.byk.com/fileadmin/BYK/downloads/supportdownloads/instruments/theory/appearance/en/Intro_Transparency.pdf

8. Thomas, J.J., et al., *A comparative study on the optical limiting properties of different nano spinel ferrites with Z-scan technique.* Materials Research Bulletin, 2012. **47**(8): p. 1855-1860.

9. Bravo, J., *Tecnologia de Polimeros y Compuestos*, in *Tipos de Polimeros*2008, Universidad Carlos III de Madrid. p. 34.

10. Sreejarani Kesavan Pillai, S.S.R., *Chitosan-based Nanocomposites*, in *Natural polymers, volume 2: nanocomposites*, M.J.J.a.T. Sabu, Editor. 2012, The Royal Society of Chemistry p. 35.

11. Manuel Billón Timón, R.v.G.L., *Aplicaciones de las ferritas magneticas blandas*, 2007, Universidad Carlos III de Madrid. p. 51.

12. Šepelák, V., et al., *Evolution of structure and magnetic properties with annealing temperature in nanoscale high-energy-milled nickel ferrite.* Journal of Magnetism and Magnetic Materials, 2003. **257**(2–3): p. 377-386.

13. Nathani, H., S. Gubbala, and R.D.K. Misra, *Magnetic behavior of nickel ferrite-polyethylene nanocomposites synthesized by mechanical milling*

process. Materials Science and Engineering B-Solid State Materials for Advanced Technology, 2004. **111**(2-3): p. 95-100.

14. V. Šepelák, I.B., D. Menzel, A. Feldhoff , P. Heitjans, F. Krumeich, S. J. Campbell, and K. D. Becker, *Magnetic behavior of nanocrystalline NiFe2O4.* p. 2.

15. Rekhila, G., Y. Bessekhouad, and M. Trari, *Visible light hydrogen production on the novel ferrite NiFe2O4.* International Journal of Hydrogen Energy, 2013. **38**(15): p. 6335-6343.

16. Nathani, H. and R.D.K. Misra, *Surface effects on the magnetic behavior of nanocrystalline nickel ferrites and nickel ferrite-polymer nanocomposites.* Materials Science and Engineering: B, 2004. **113**(3): p. 228-235.

17. An-Hui Lu, E.L.S.a.F.S., *Magnetic nanoparticles: Synthesis, Protection, Functionalization, and Application.* Wiley-VCH Verlag GmbH & Co., 2007: p. 23.

18. (ICBA), I.c.b.a. *General information of Carbon black.* 2012 August, 3rd 2013].

19. Mansour, K., M.J. Soileau, and E.W.V. Stryland, *Nonlinear optical properties of carbon-black suspensions (ink).* J. Opt. Soc. Am. B, 1992. **9**(7): p. 1100-1109.

20. Mansour, K., E.W. Van Stryland, and M.J. Soileau. *Optical nonlinearities in carbon black particles*. 1990.

21. O. Durand, P.B., V. Grolier-Mazza, *Nonlinear scattering in carbon black suspensions for optical limiting*, in *Cleo*1997. p. 1.

22. Jäger, C., et al., *Spectral properties of carbon black.* Journal of Non-Crystalline Solids, 1999. **258**(1–3): p. 161-179.

23. Hossain, M.K., *Scanning Electron Microscopy Study of Fiber reinforced Polymeric Nanocomposites.* Scanning Electron Microscopy by Dr. Viacheslav Kazmiruk, 2012: p. 13.

24. Xi Xu, Q.W., Xiangan Kong, Xiaodong Zhang and Jingui Huang, *Pan mill type equipment designed for polymer stress reactions: Theoretical analysis of structure and milling process of equipment.* Plastics Rubber and Composites Processing and Applications, 1996. **25 (3)**: p. 152-158.

25. Lu, C.H. and Q. Wang, *Preparation of ultrafine polypropylene/iron composite powders through pan-milling.* Journal of Materials Processing Technology, 2004. **145**(3): p. 336-344.

26. Smith, A.P., et al., *High-energy mechanical milling of poly(methyl methacrylate), polyisoprene and poly(ethylene-alt-propylene).* Polymer, 2000. **41**(16): p. 6271-6283.

27. Linde North America, I., *Cryogenic grinding. Fine particle pulverization with Nitrogen or Carbon Dioxide.* 2013: p. 2.

28. A.P. Smith, H.A., C.C. Koch, R.J. Spontak, *Cryogenic mechanical alloying as an alternative strategy for the recycling of tires.* polymer 2000. **42**: p. 4453-4457.

29. Srinivas Jonna, J.L., *Processing and properties of cryogenically milled post-consumer mixed plastic waste.* Polymer testing, 2005. **24**: p. 428-434.

30. Silvina P. Limandri, A.C.C., and Jorge C. Trincavelli, *Effects of the Carbon Coating and the Surface Oxide Layer in Electron Probe Microanalysis.* Microscopy and Microanalysis, 2010. **16**: p. 583-593.

31. Kotál, V., et al., *Gold Coating of Poly(ethylene terephthalate) Modified by Argon Plasma.* Plasma Processes and Polymers, 2007. **4**(1): p. 69-76.

32. M. Rubin, C.B.H.a.N.-H.-C., *Optical and Mechanical Properties of D.C. Sputtered Carbon Films.* p. 18.

33. Huang, M., et al., *Graphite-like carbon films by high power impulse magnetron sputtering.* Applied Surface Science, (0).

34. Hein, L.R.O., et al., *A Brief Discussion About Image Quality and SEM Methods for Quantitative Fractography of Polymer Composites.* Scanning, 2013. **35**(3): p. 196-204.

8 Appendix

A) Poly methyl methacrylate properties from *Lucite international Co*

Property	Test method	Units	Value
THERMAL			
-Melt flow index	ISO 1133	Gms/10mins	4,4
-Vicat softening point	ISO 306A	ºC	113
	ISO 306B	ºC	106
-Heat deflection temperature	ISO 75A	ºC	99
	ISO 75B	ºC	102
-Coefficient of expansion	ASTM E831	ºC	
OPTICAL			
-Light transmission	ASTM D1003	%	92
-Haze	ASTM D1003	%	0,4
-Refractive index	ISO 489	-	1,49
MECHANICAL			
-Tensile strength	ISO 527	MPa	80
-Elongation	ISO 527	%	5
-Flexural modulus	ISO 178	GPa	3,2
-Flexural strength	ISO 178	MPa	110
-Izod impact strength	ISO 180/1A	Kj/m^2	1,8
-Charpy impact strength	ISO 179/1eA	Kj/m^2	2
	ISO 179/1Eu	Kj/m^2	18
GENERAL			
-Relative density	ISO 1183	-	1,18
-Rockwell hardness	ISO 2039-2	M Scale	98
-Ball indentation hardness	ISO 2039-1	MPa	185
	(H 961/30)		
-Mould shrinkage	-	%	0,4-0,7
-Water absorption	ISO 62	%	0,3
-Flammability	UL94	-	HB
-Glow wire test	IEC 695-2-1	º C	650

B) Nickel iron oxide from *NanoAmor Nanostructured & Amorphous Materials, Inc.*

Property	Units	Value
Purity	%	98
Average particle size (APS)	nm	20-30
Specific Surface Area (SSA)	m^2/g	59
Color	-	Dark brown
Morphology	-	Nearly spherical
Bulk density	g/cm^3	0,89
True density	g/cm^3	5,368

C) SEM images from the different mechanical alloying process.

- **Process A (Alumina container with alumina balls)**
  - **Sample P1610**

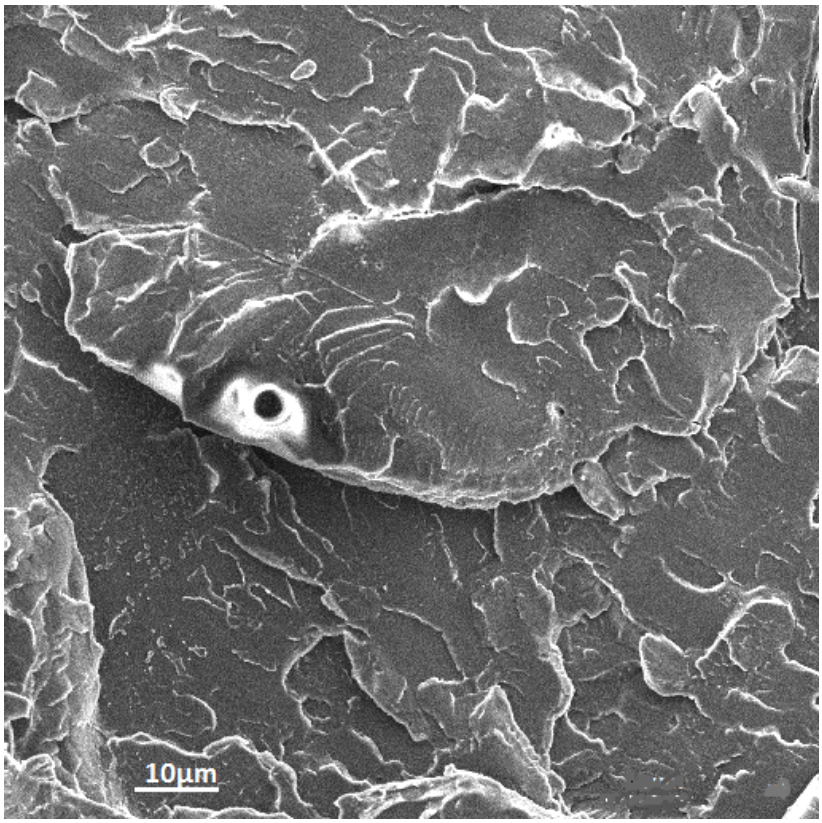

Figure 10: P1610 → Beam voltage: 5 kV & Working distance: 7mm.

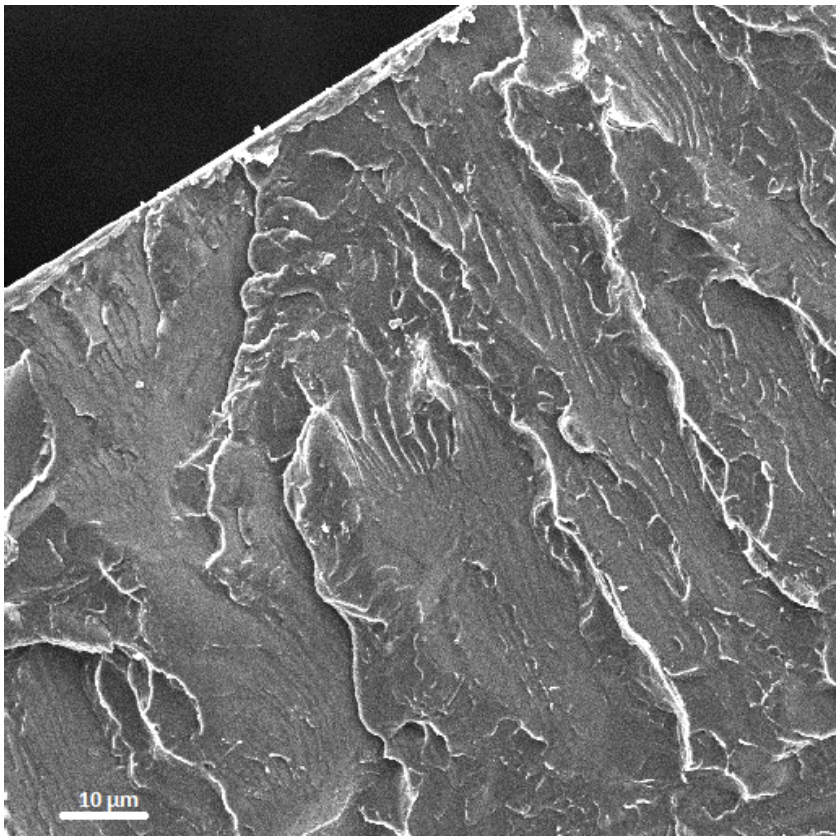

Figure 11: P1610→ Beam voltage: 5 kV& Working distance: 7 mm..

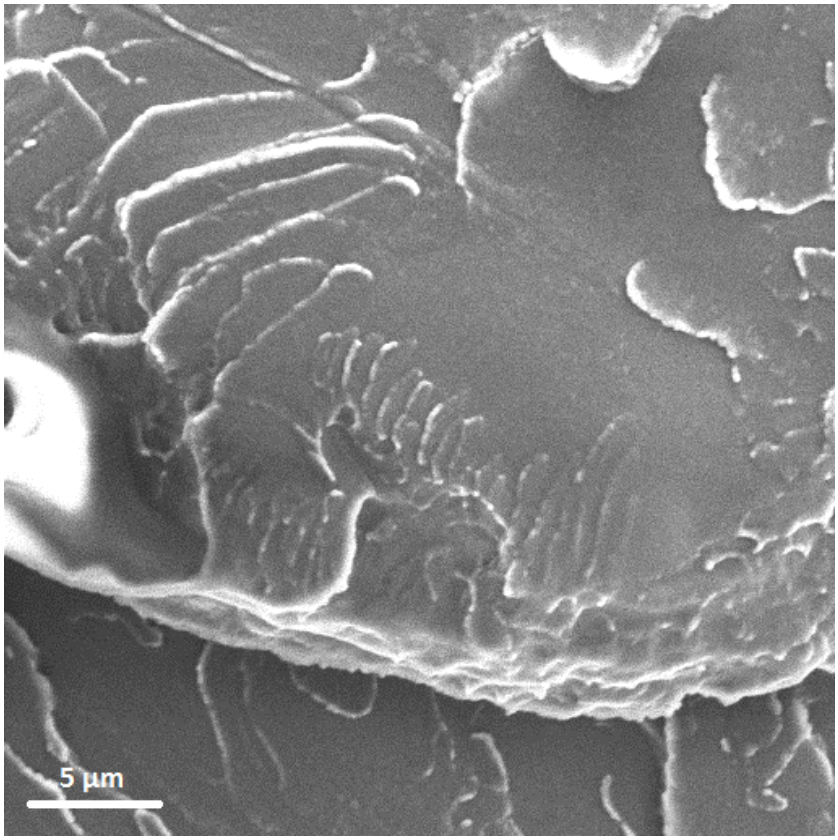

Figure 12: P1610→ Beam voltage: 5 kV & Working distance: 7 mm.

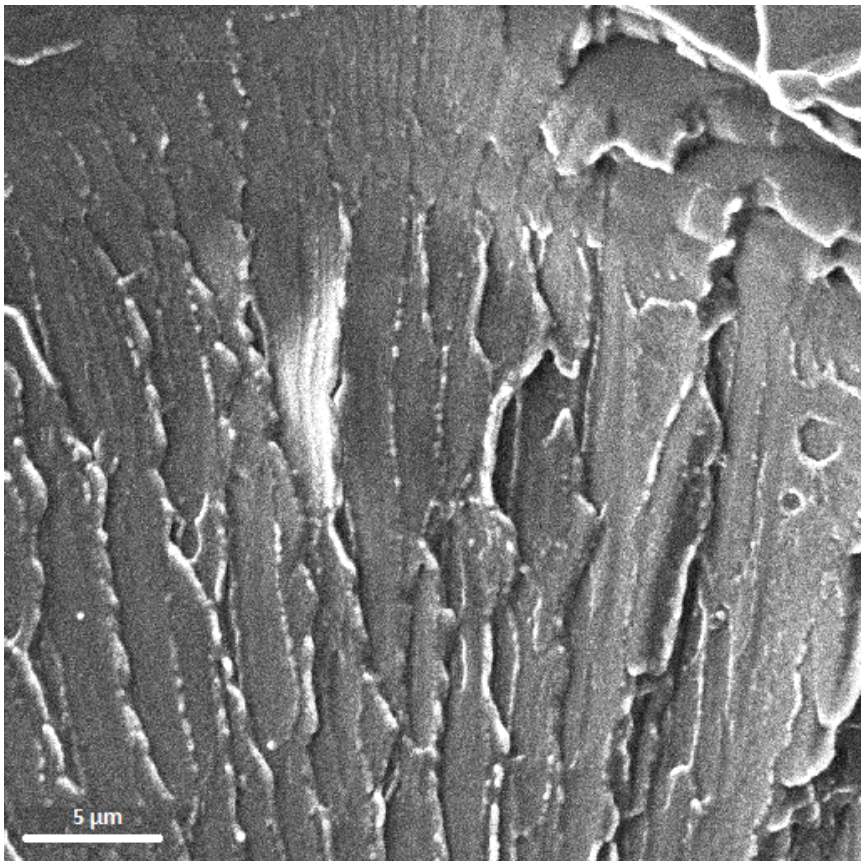

Figure 13: P1610→Beam voltage: 5 kV & Working distance: 5 mm.

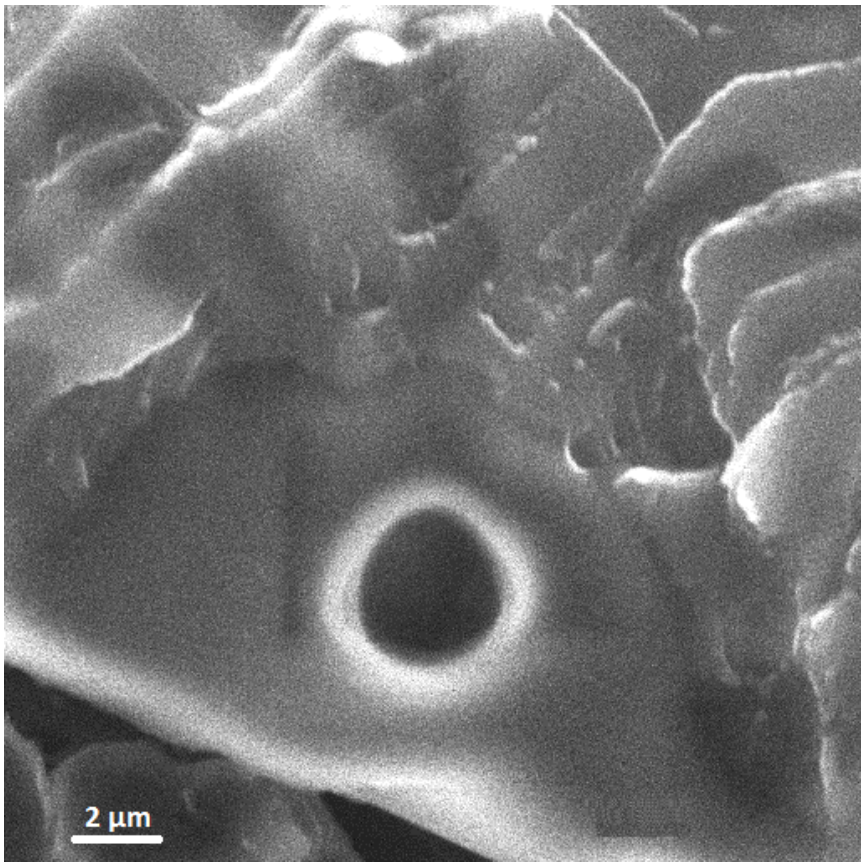

Figure 14: P1610→Beam voltage: 10 kV & Working distance: 7 mm.

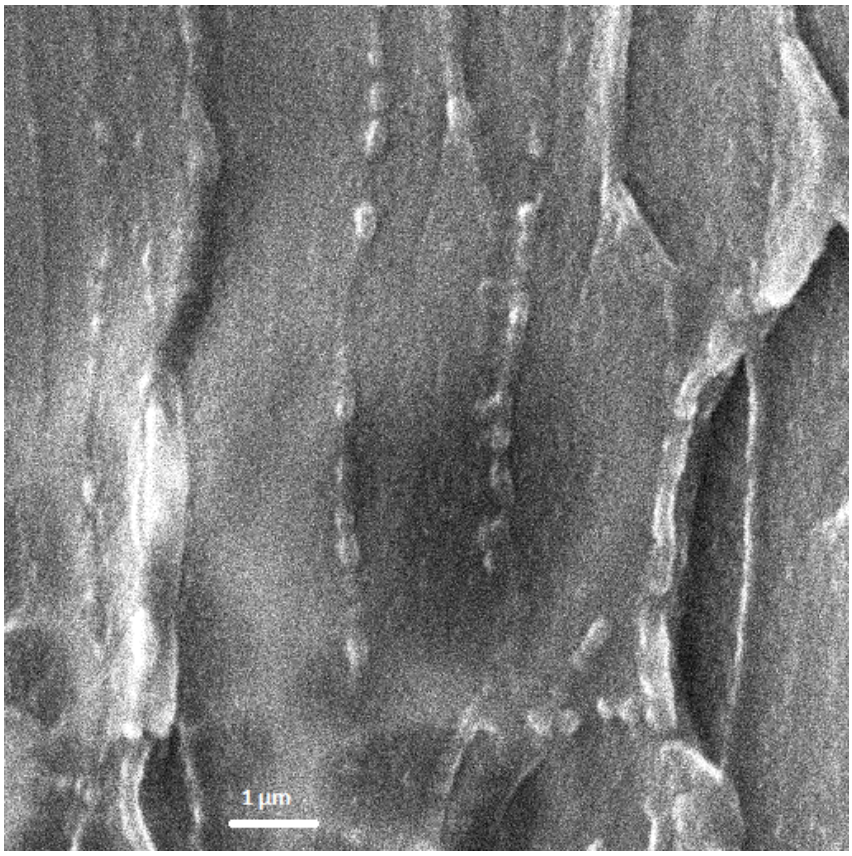

Figure 15: P1610→Beam voltage: 10 kV & Working distance: 5 mm.

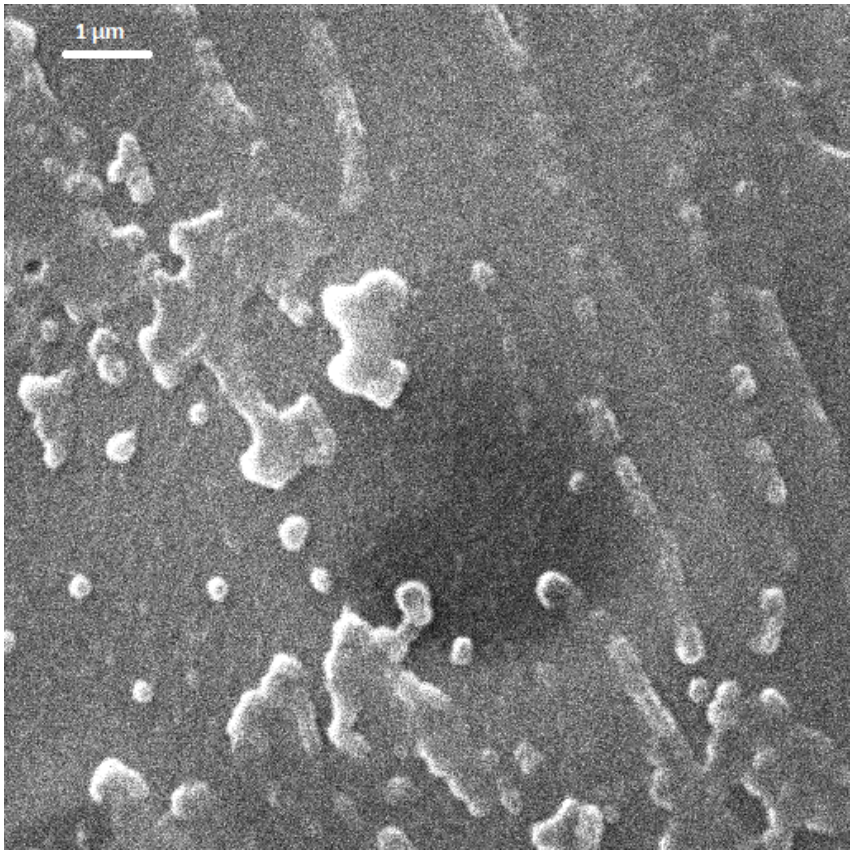

Figure 16: P1610→Beam voltage: 10 kV & Working distance: 5mm.

- **P1610 without a proper time in the liquid nitrogen**

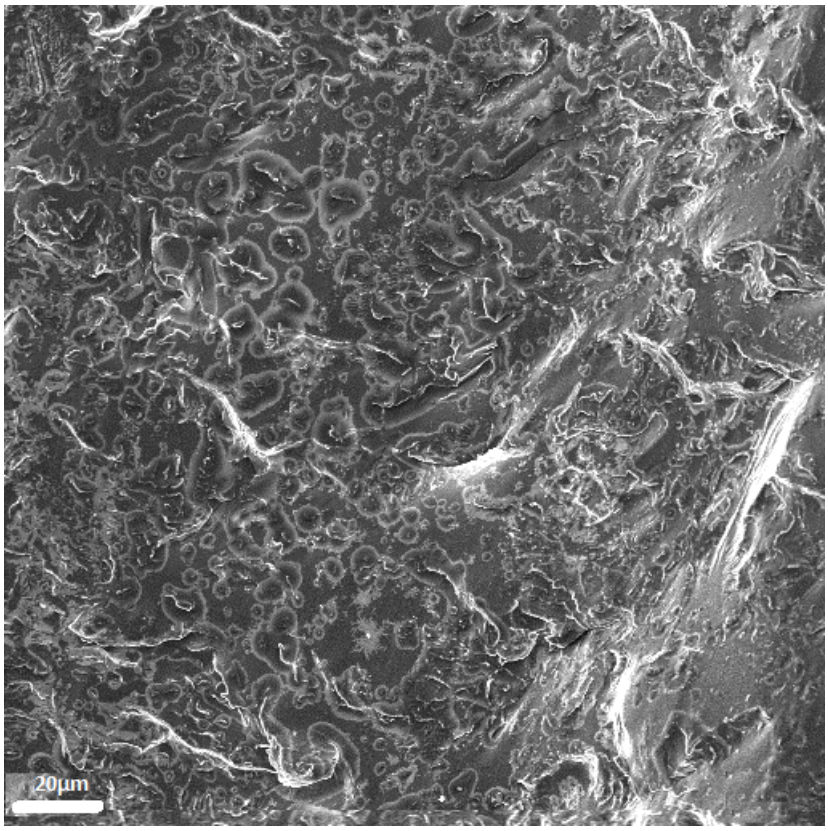

Figure 17: P1610→Beam voltage: 5 kV & Working distance: 12 mm..

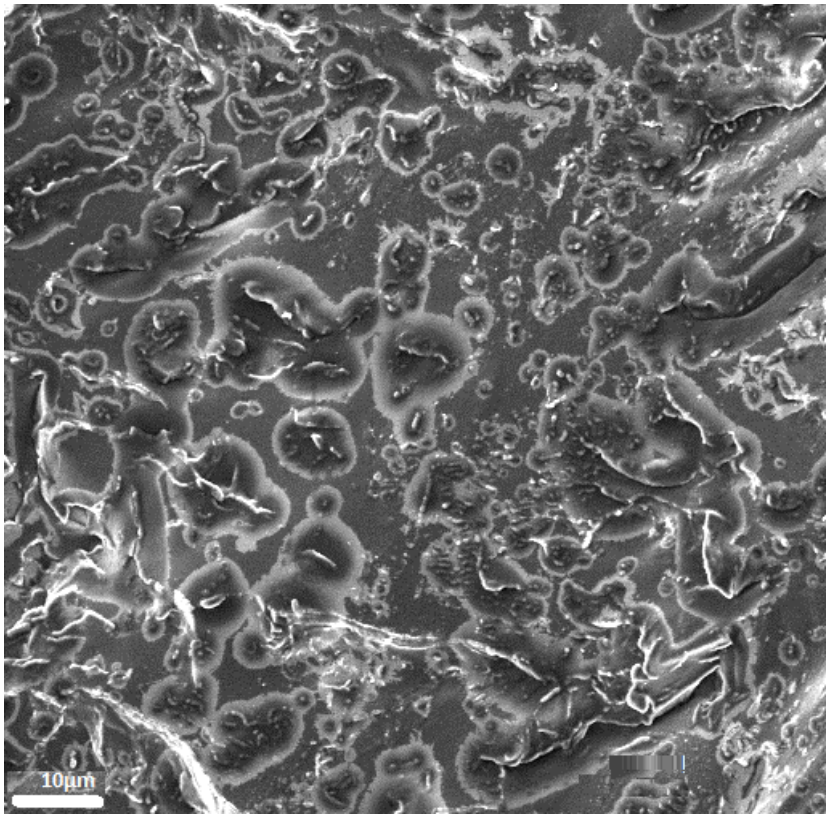

Figure 18: P1610→Beam voltage: 5 kV & Working distance: 12mm..

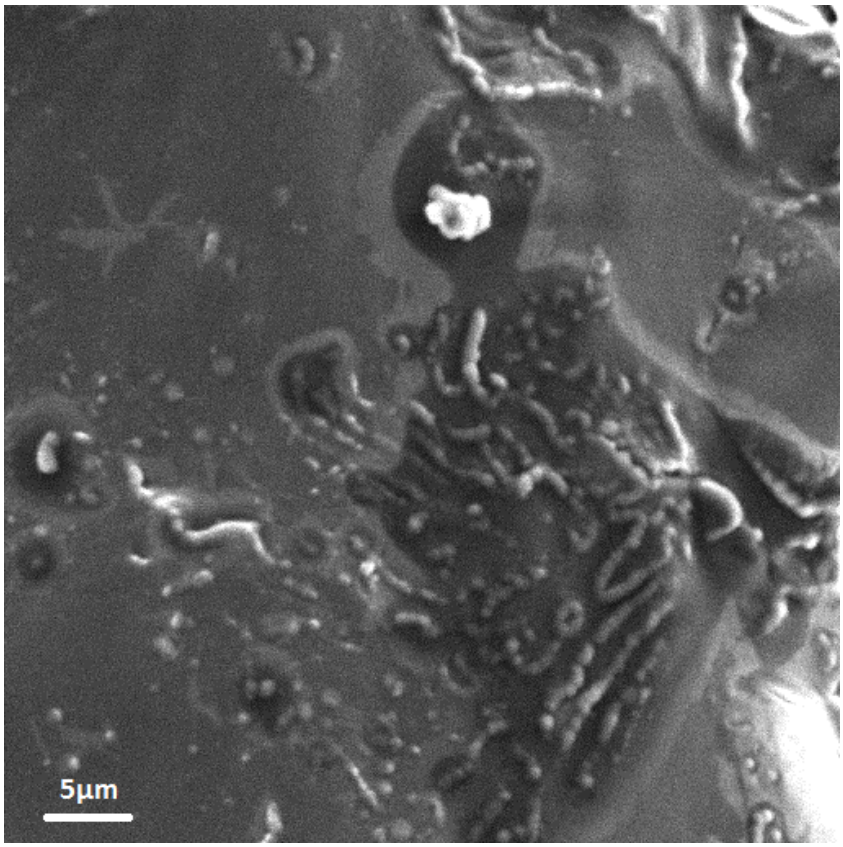

Figure 19: P1610→Beam voltage: 5kV& Working distance: 11 mm.

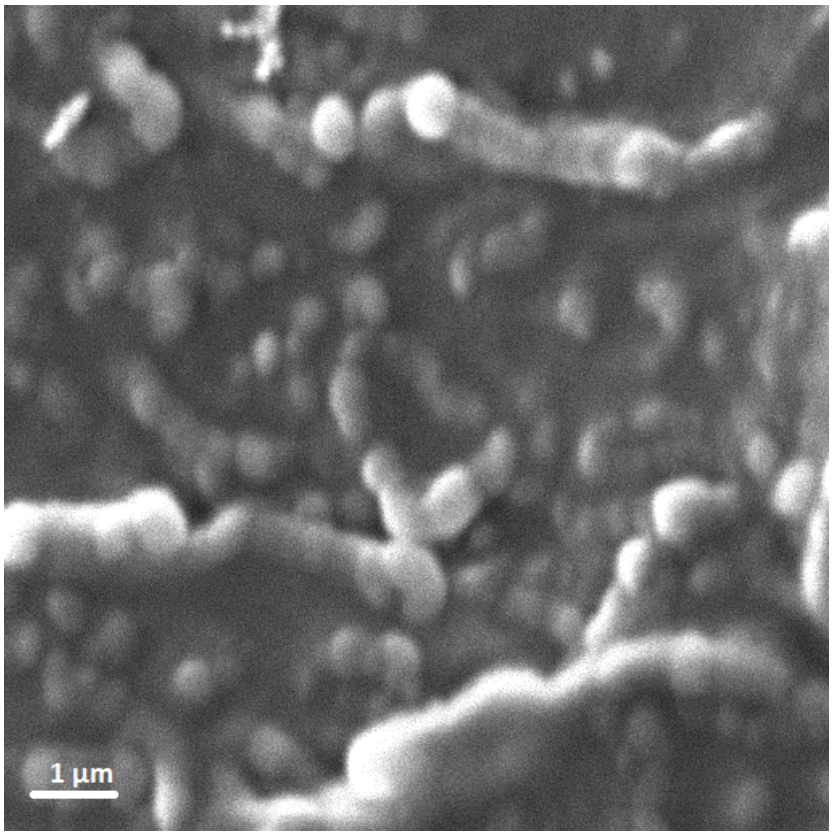

Figure 20: P1610→Beam voltage: 5 kV & Working distance: 7 mm..

- **P1605**

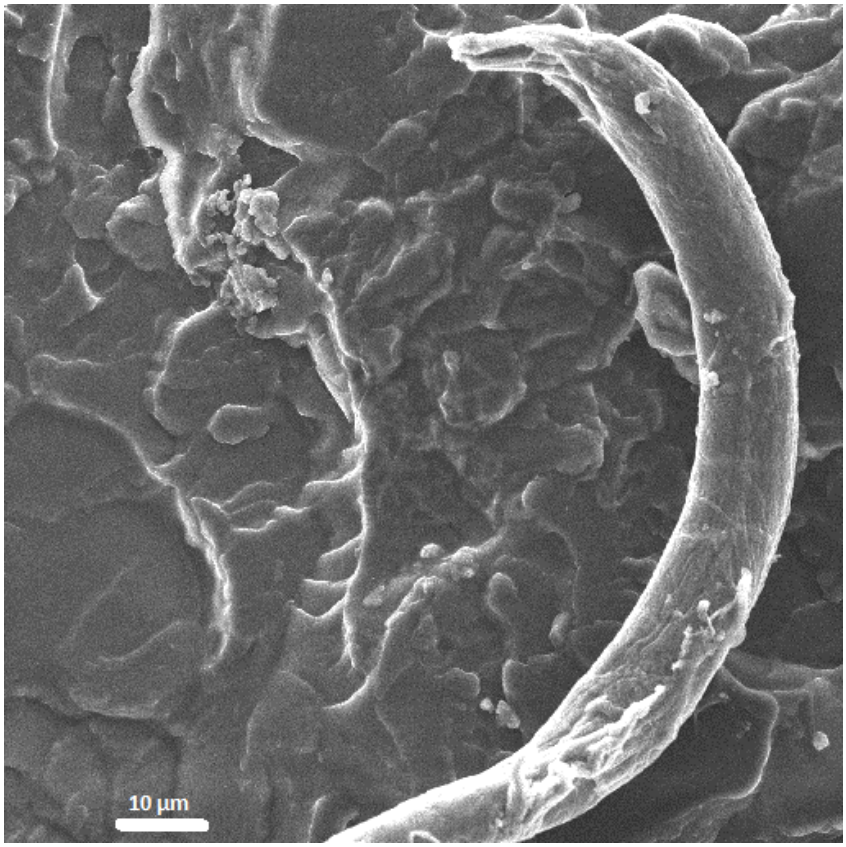

Figure 3: P1605→Beam voltage: 10kV & Working distance: 5mm.

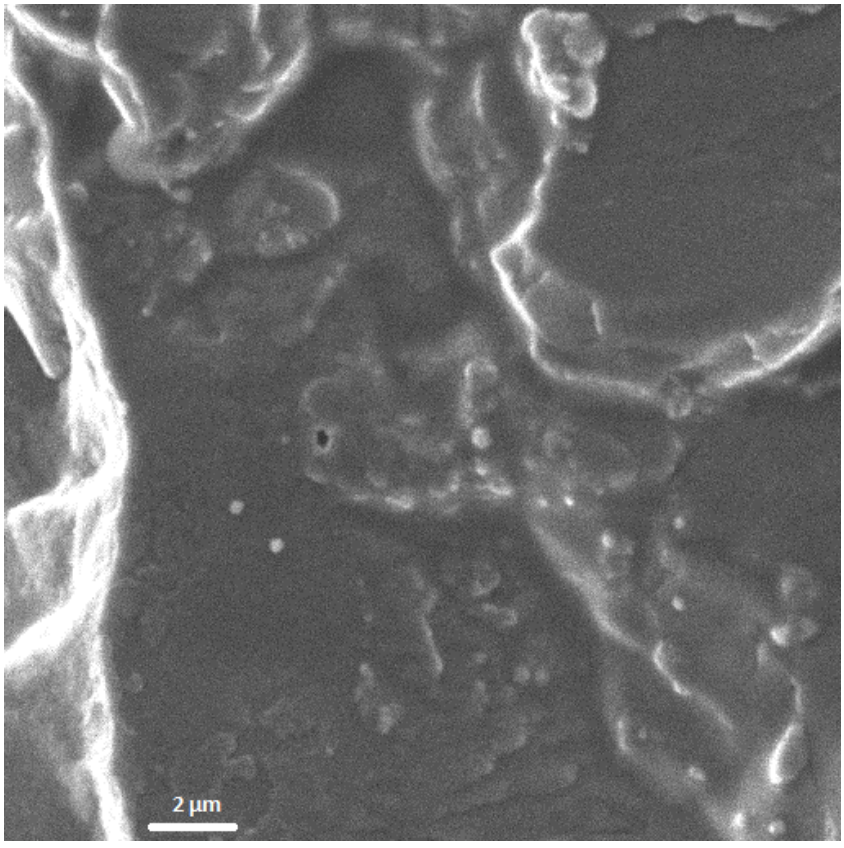

Figure 4: P1605→Beam voltage: 5kV & Working distance: 5 mm.

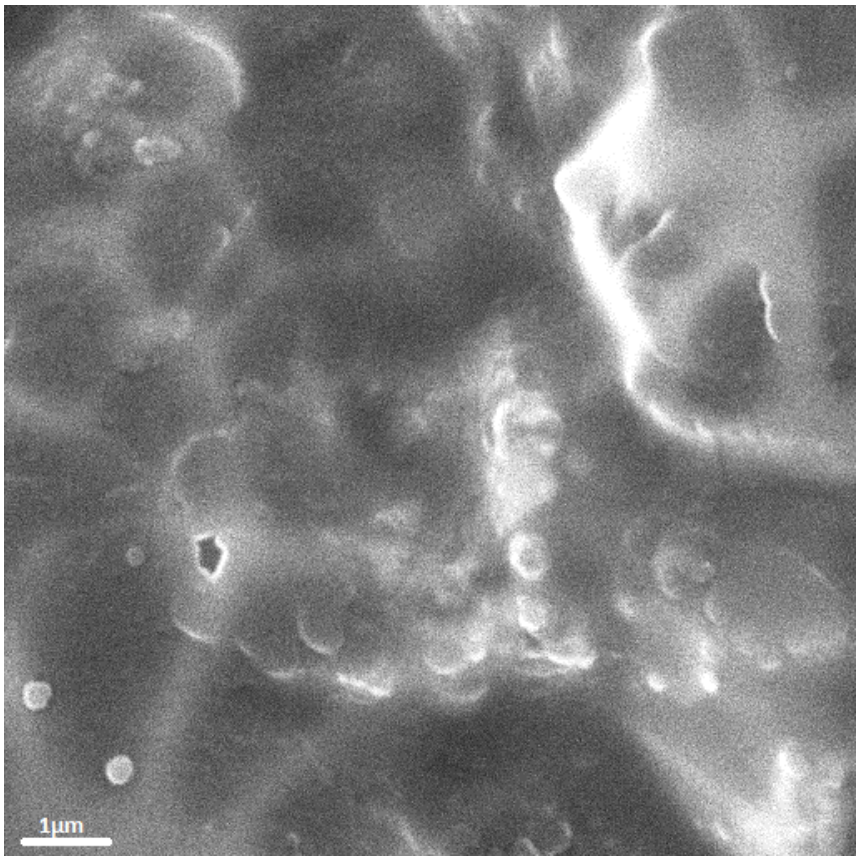

Figure 5: P1605→Beam voltage: 10 kV & Working distance: 5mm.

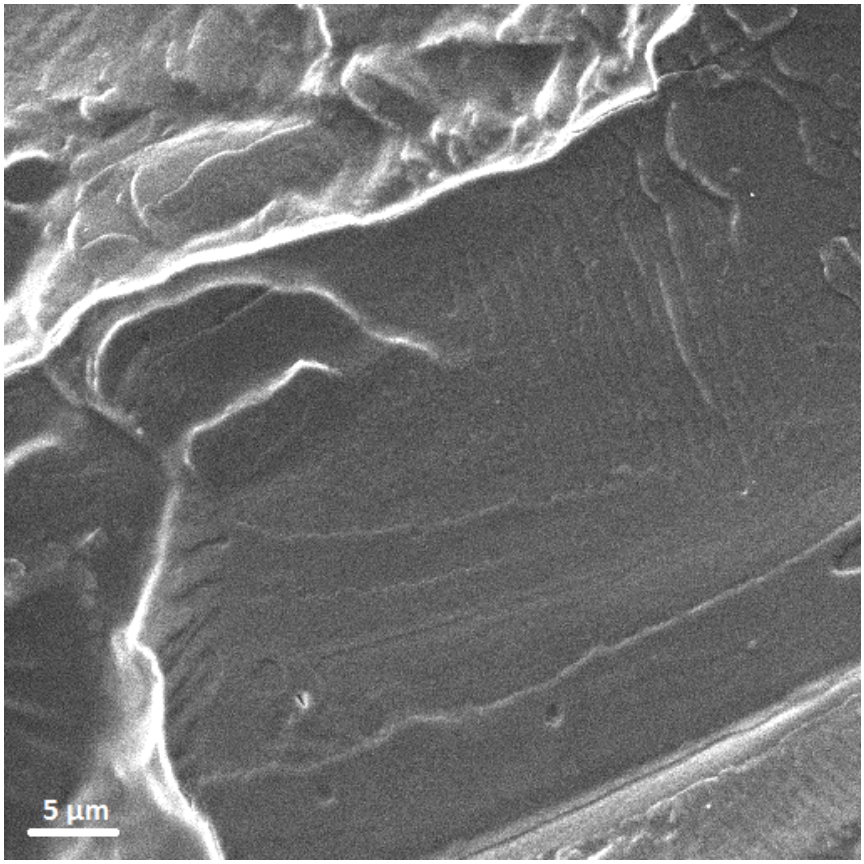

Figure 6: P1605→Beam voltage: 5 kV & Working distance: 5mm.

- **P1600**

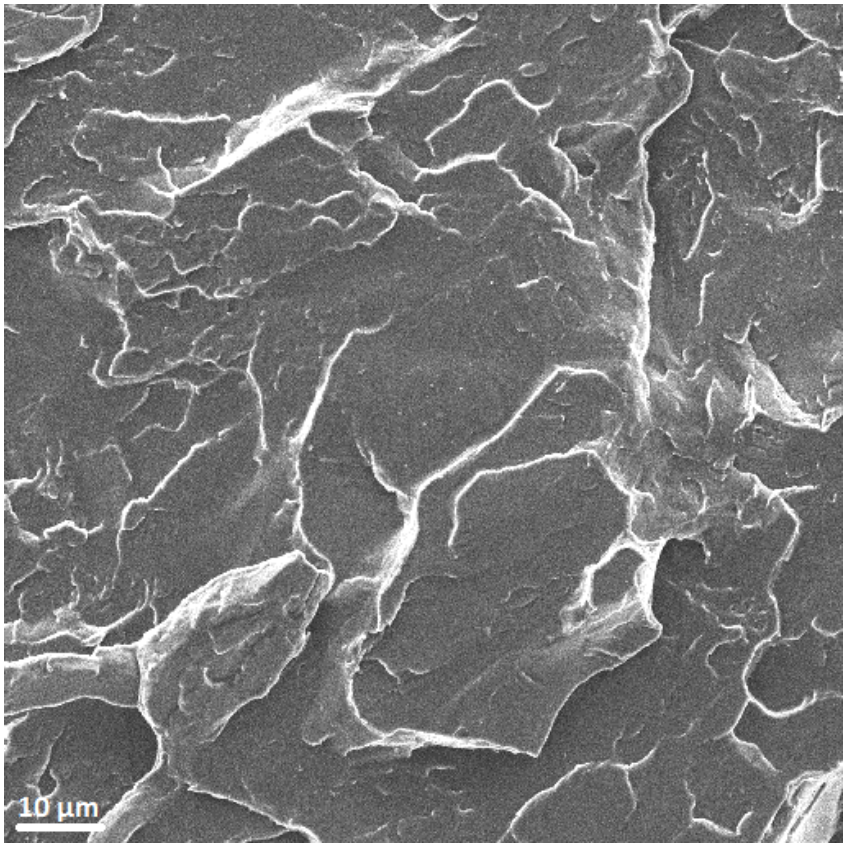

Figure 7: P1600→Beam voltage: 5 kV & Working distance: 6mm.

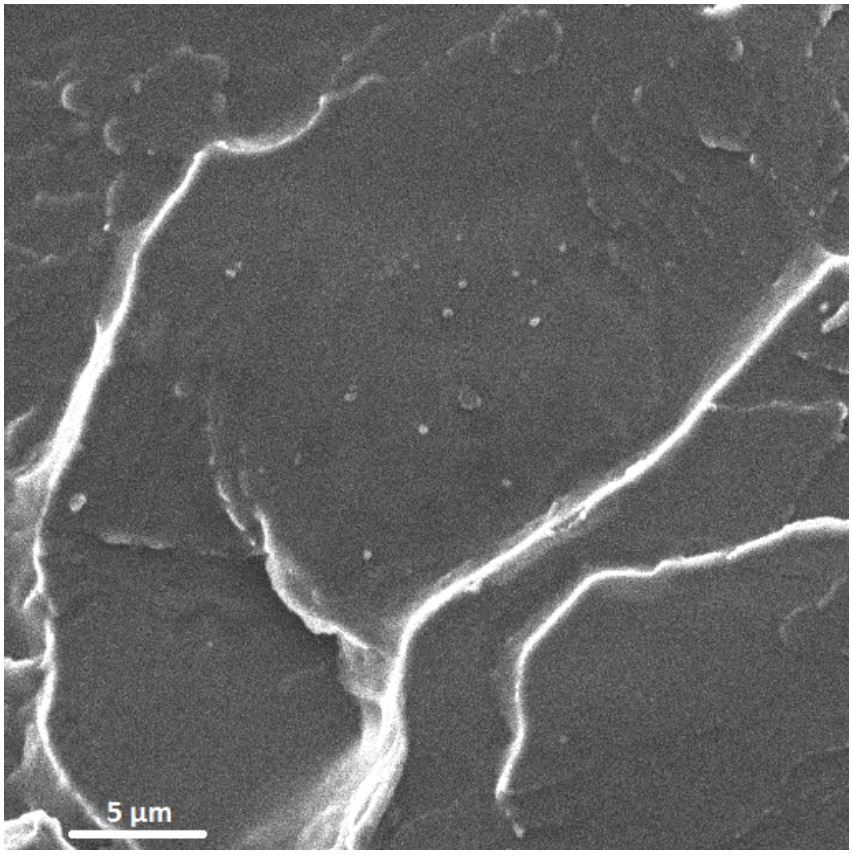

Figure 8: P1600→Beam voltage: 5kV & Working distance: 6mm.

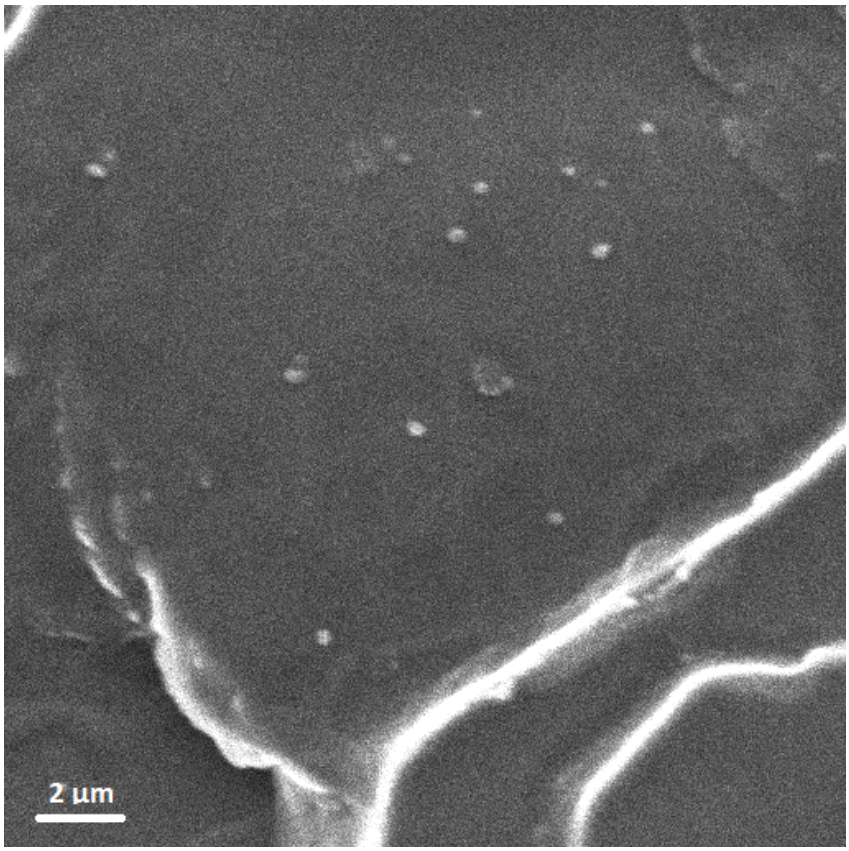

Figure 9: P1600→Beam voltage: 5kV& Working distance: 6mm.

- **G1210**

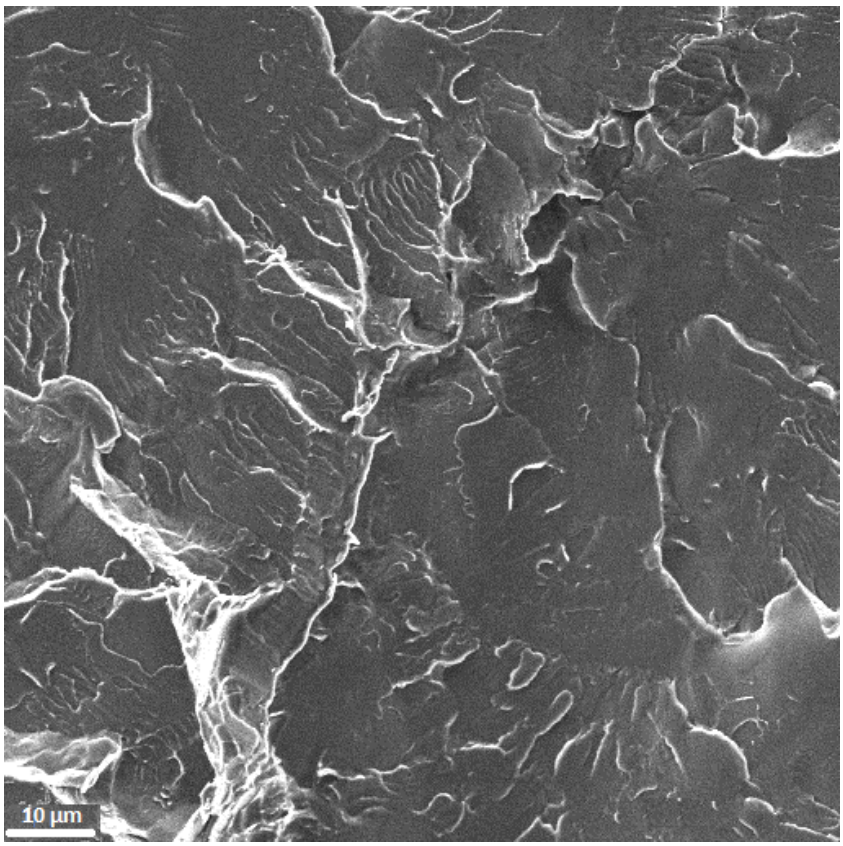

Figure 10: G1210→Beam voltage: 5kV & Working distance: 4mm.

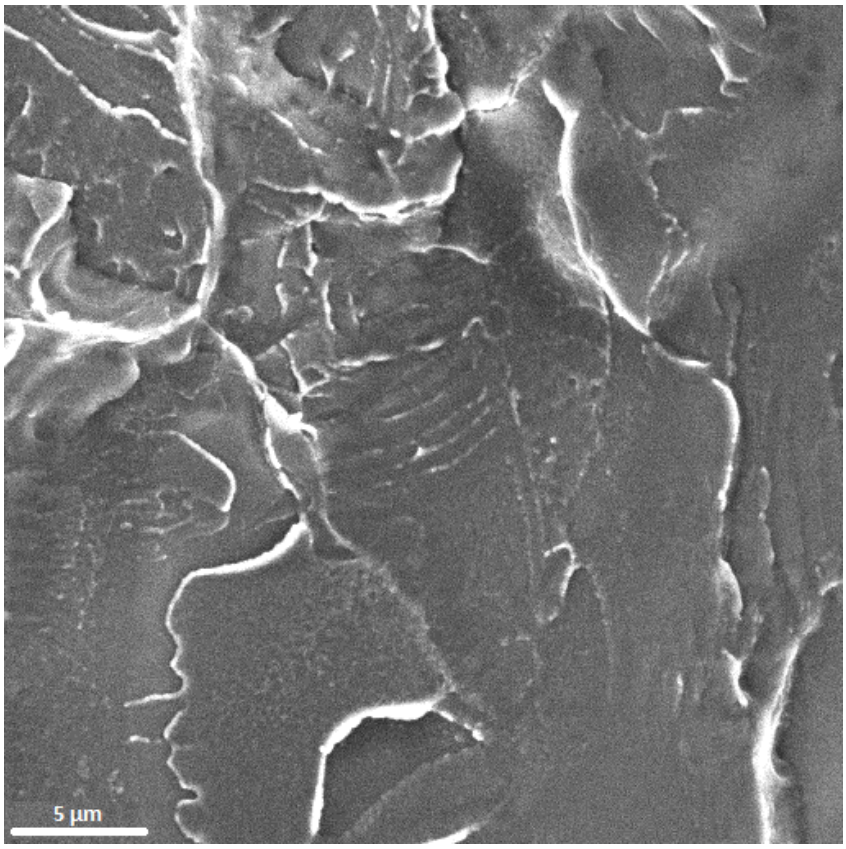

Figure 11: G1210→Beam voltage: 5kV & Working distance: 6mm.

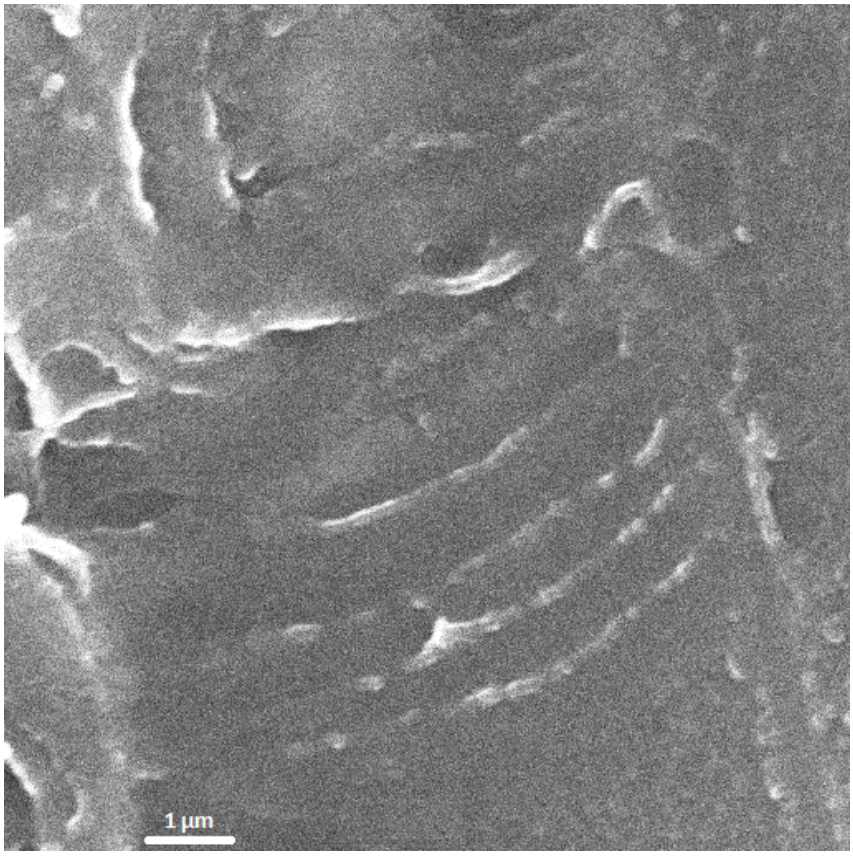

Figure 12: G1210→Beam voltage: 10kV & Working distance: 6mm.

- **G1200**

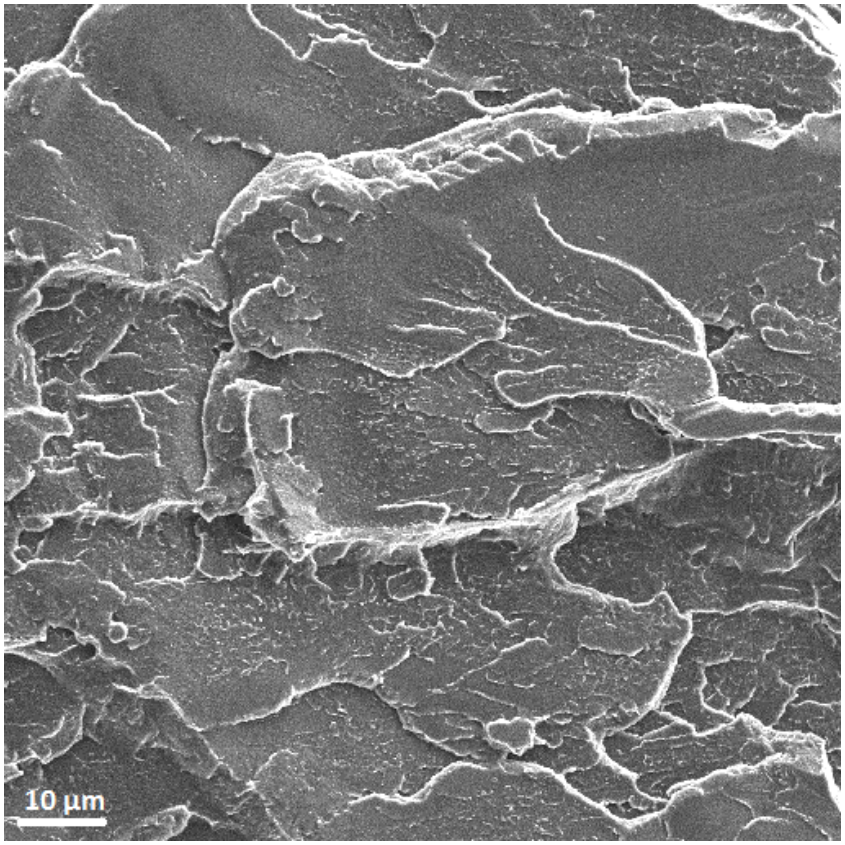

Figure 13: G1200→Beam voltage: 5kV & Working distance: 5mm.

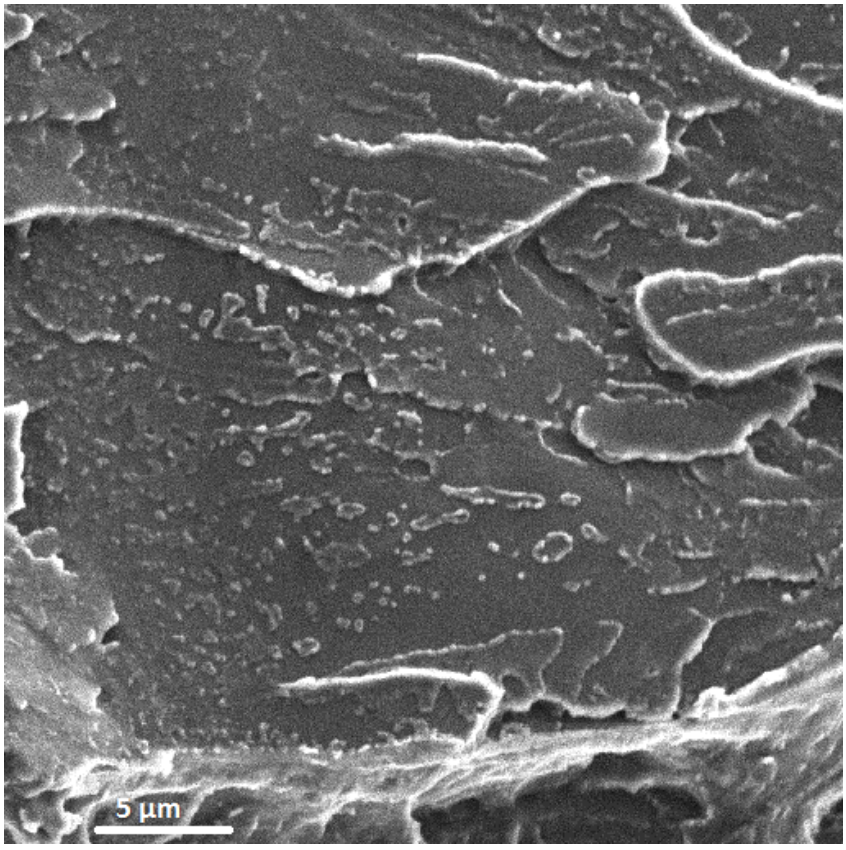

Figure 14: G1200→Beam voltage: 5kV & Working distance: 5mm.

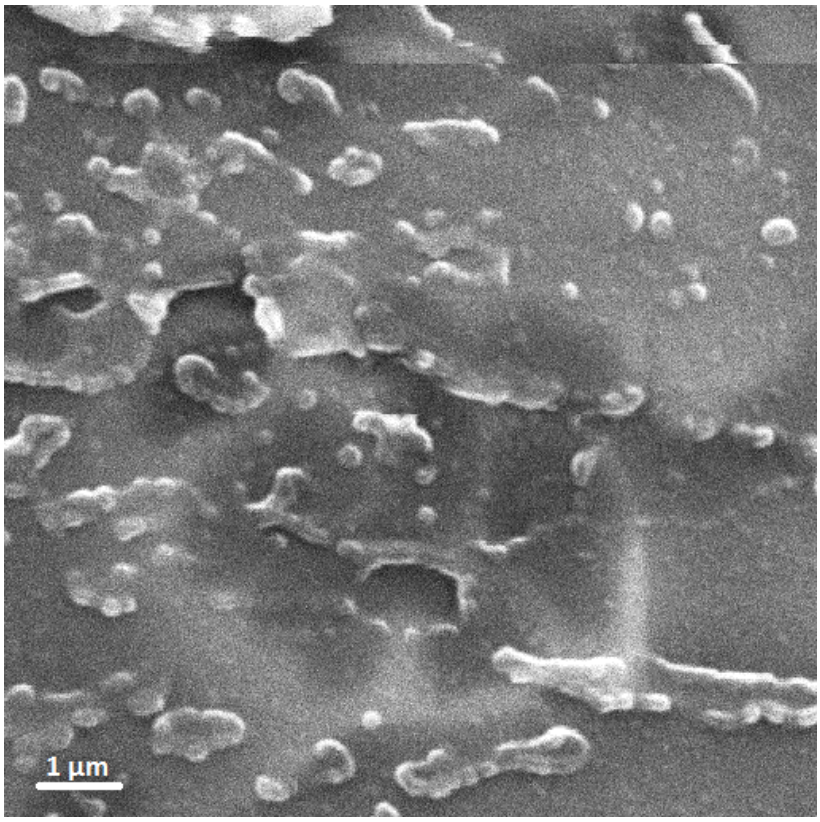

Figure 15: G1200→Beam voltage: 10kV &Working distance: 5mm.

Process B (Container with 3 steel balls):

- **$NiFe_2O_4$ 0,01% 4000s**

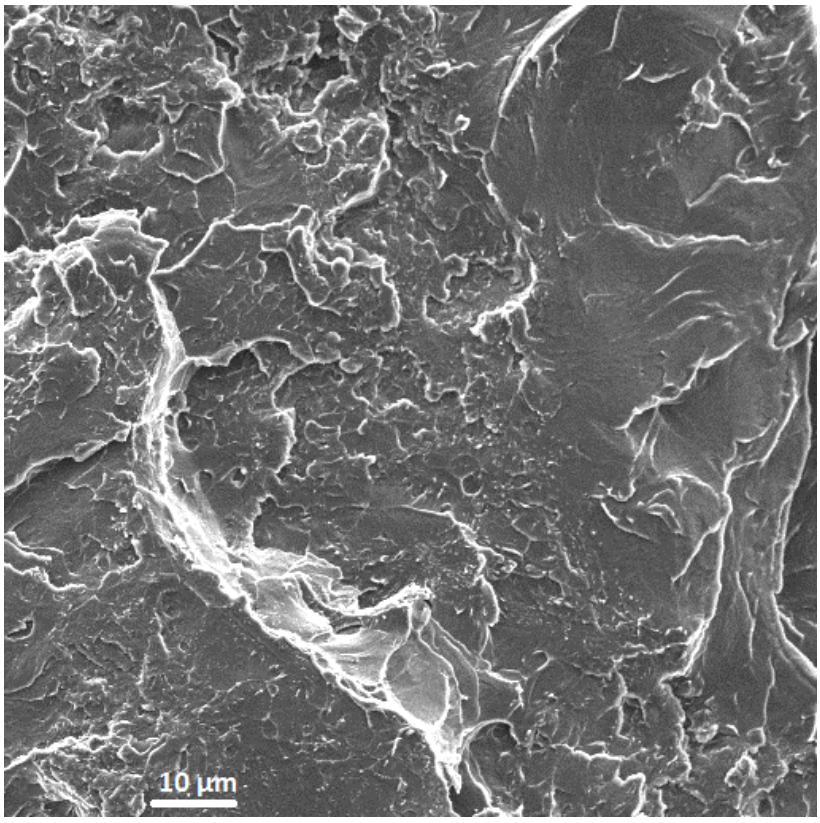

Figure 16: $NiFe_2O_4$ 0.01% 4000s→Beam voltage: 5kV & Working distance: 6mm.

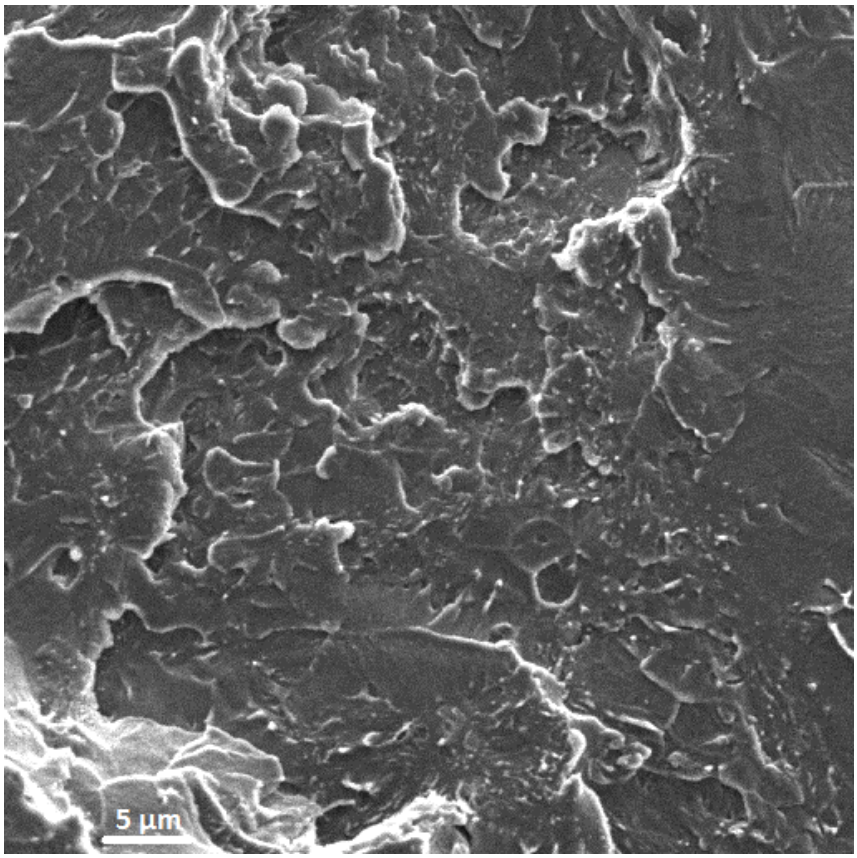

Figure 17: $NiFe_2O_4$ 0.01% 4000s→Beam voltage: 5kV & Working distance: 6mm.

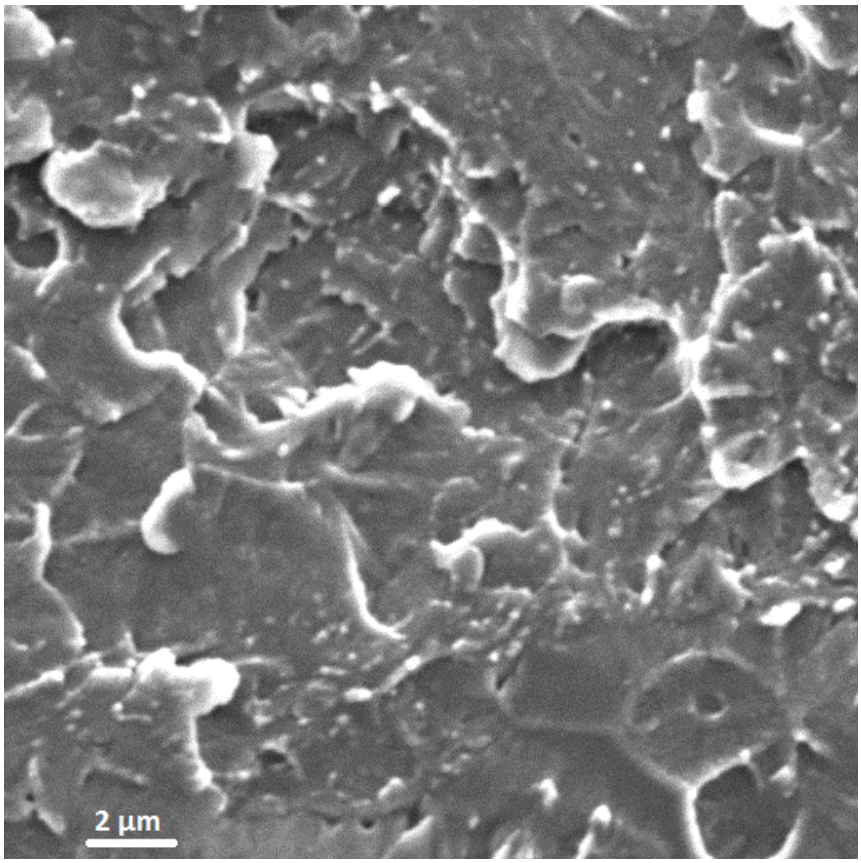

Figure 18: $NiFe_2O_4$ 0.01% 4000s→Beam voltage: 5kV & Working distance: 6mm.

- **$NiFe_2O_4$ 0,05% 4000s**

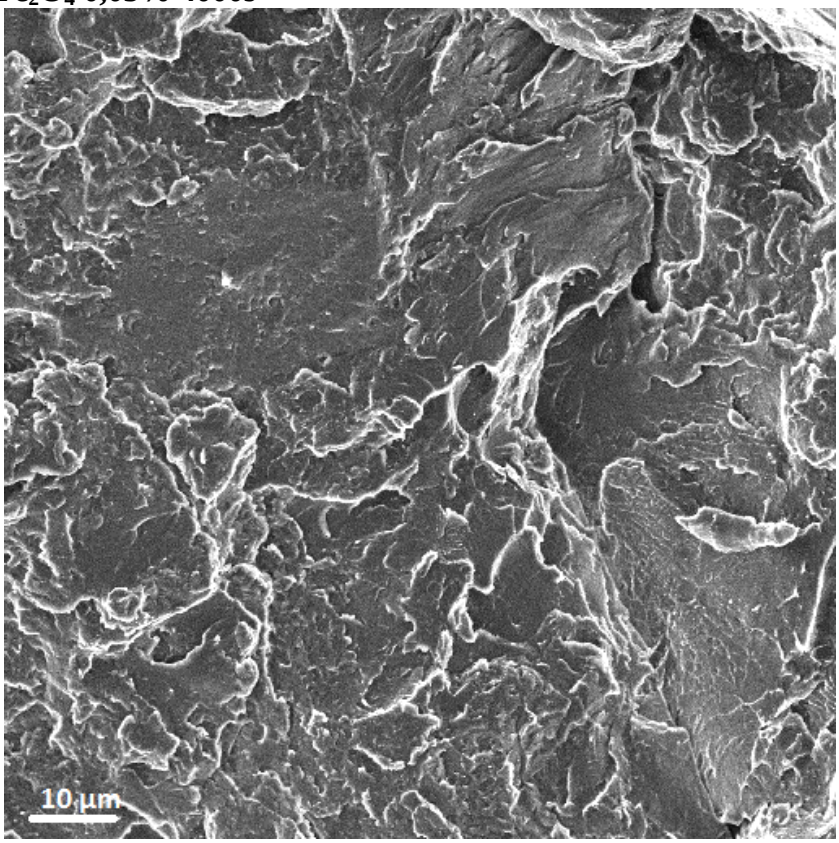

Figure 19: $NiFe_2O_4$ 0.05% 4000s→Beam voltage: 5kV & Working distance: 6mm.

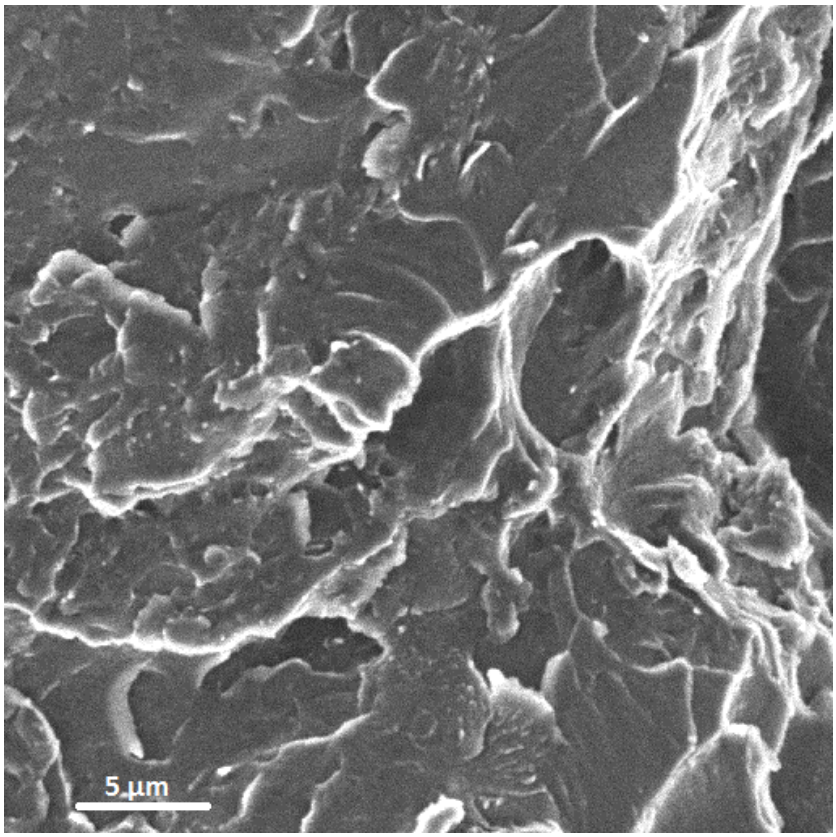

Figure 20: $NiFe_2O_4$ 0.05% 4000s→Beam voltage: 5kV & Working distance: 6mm.

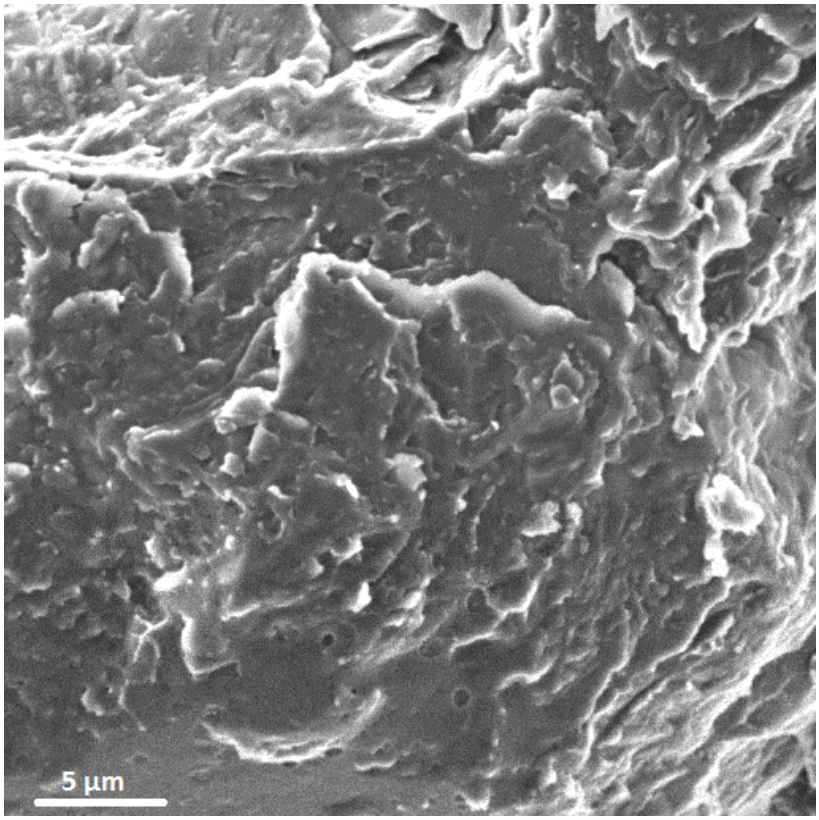

Figure 21: $NiFe_2O_4$ 0.05% 4000s→Beam voltage: 5kV & Working distance: 6mm.

- **$NiFe_2O_4$ 0,01% 6000s**

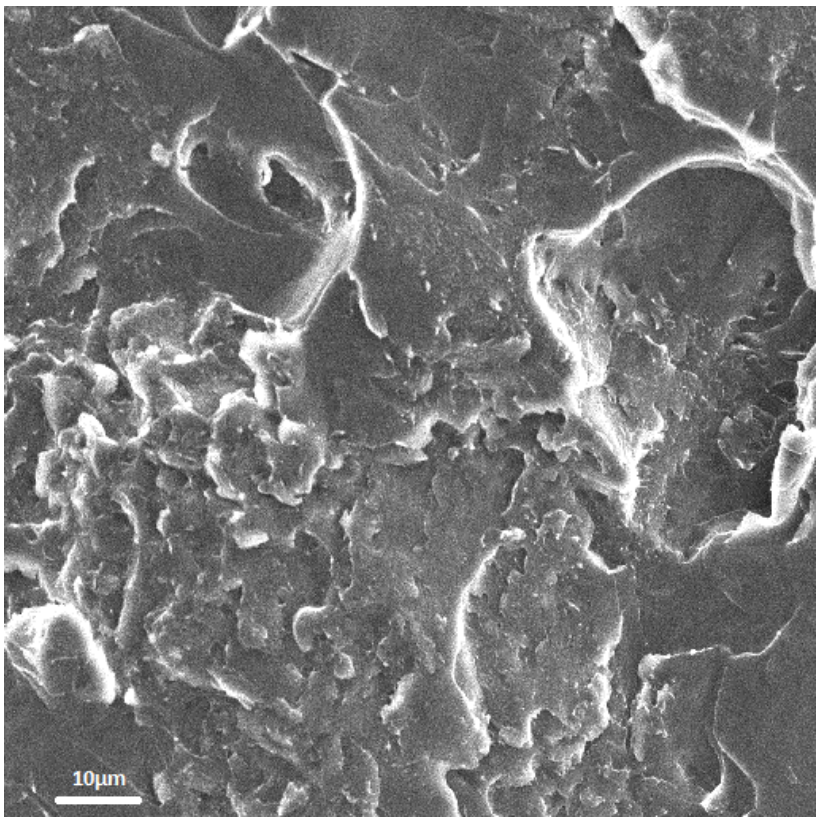

Figure 22: $NiFe_2O_4$ 0.01% 6000s→Beam voltage: 10kV & Working distance: 7mm.

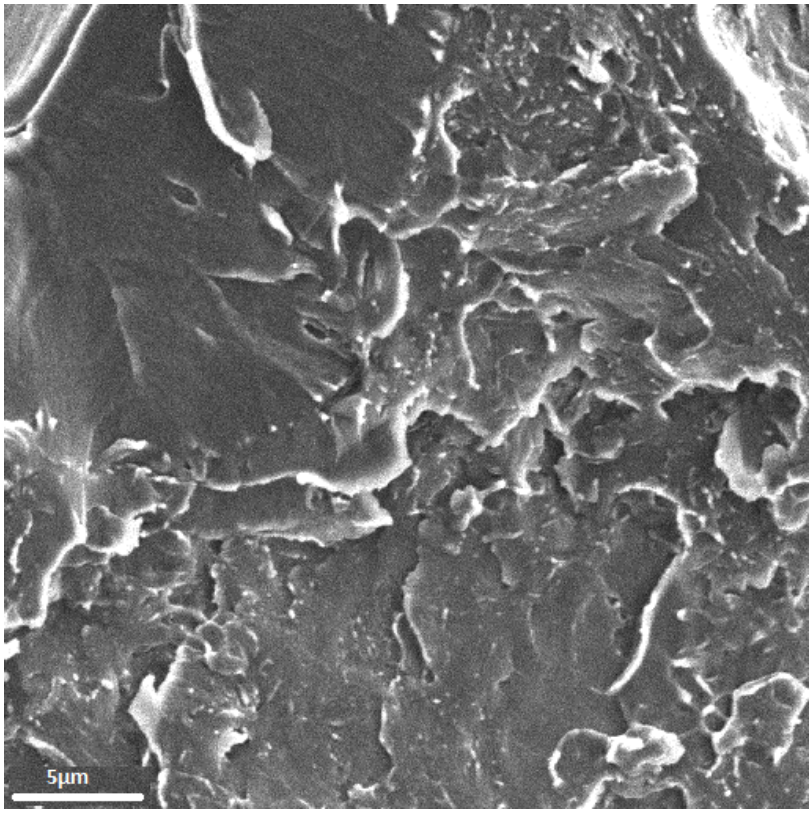

Figure 23: $NiFe_2O_4$ 0.01% 6000s→Beam voltage: 5kV & Working distance: 7mm.

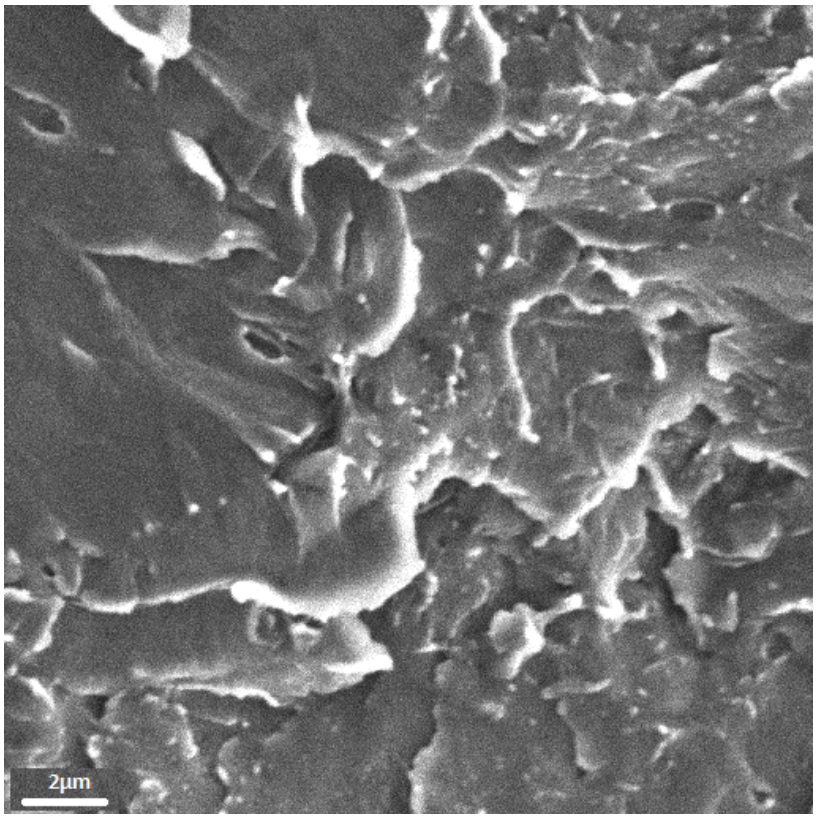

Figure 24: $NiFe_2O_4$ 0.01% 6000s→Beam voltage: 5kV & Working distance: 7mm.

- **Carbon black 0,01% 12000s**

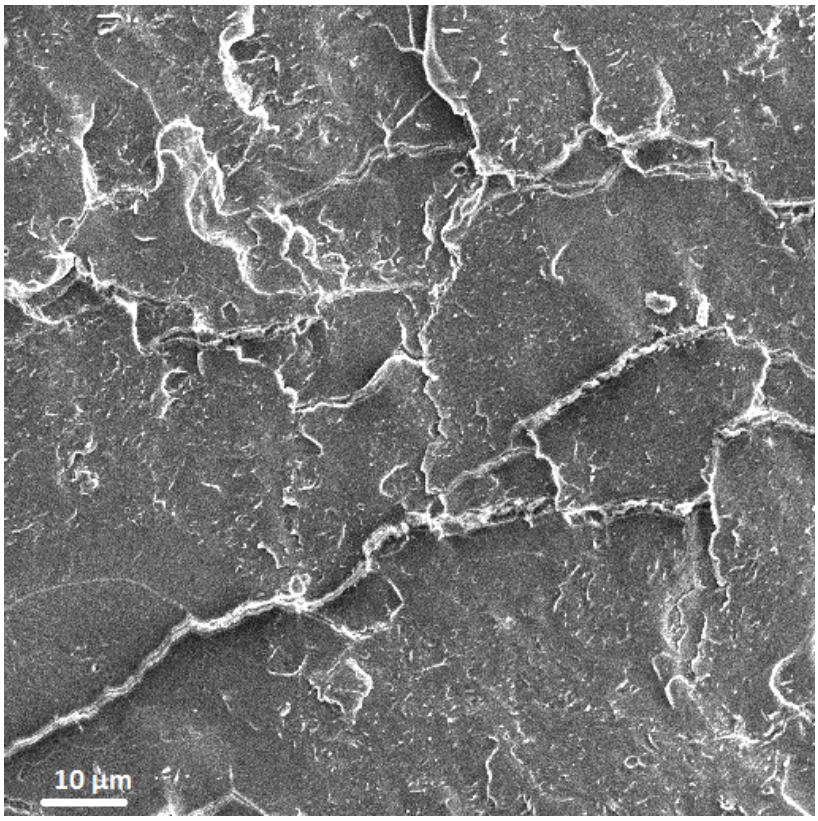

Figure 25: Carbon black 0.01% 12000s→Beam voltage: 5kV & Working distance: 7mm.

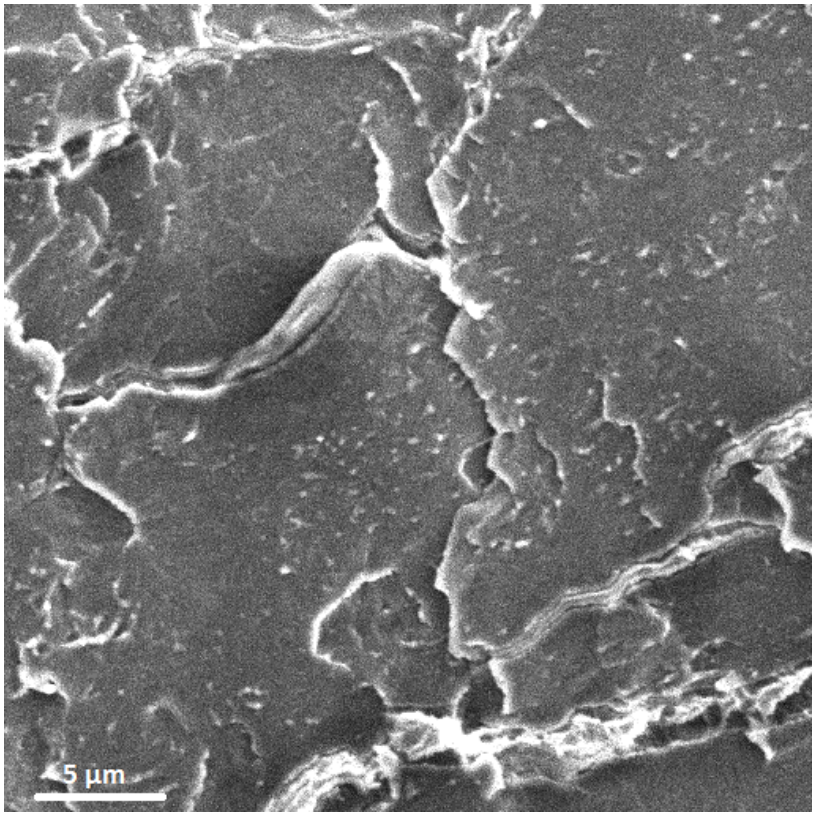

Figure 26: Carbon black 0.01% 12000s→Beam voltage: 5kV & Working distance: 7mm.

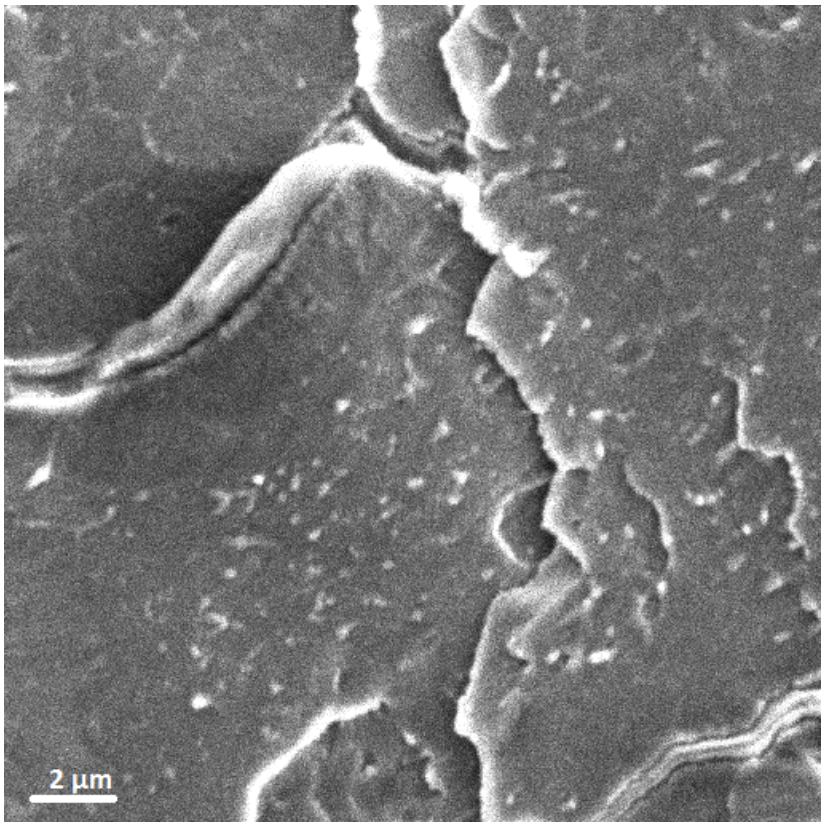

Figure 27: Carbon black 0.01% 12000s→Beam voltage: 5kV & Working distance: 7mm.

- **Carbon black 0,005% 12000s**

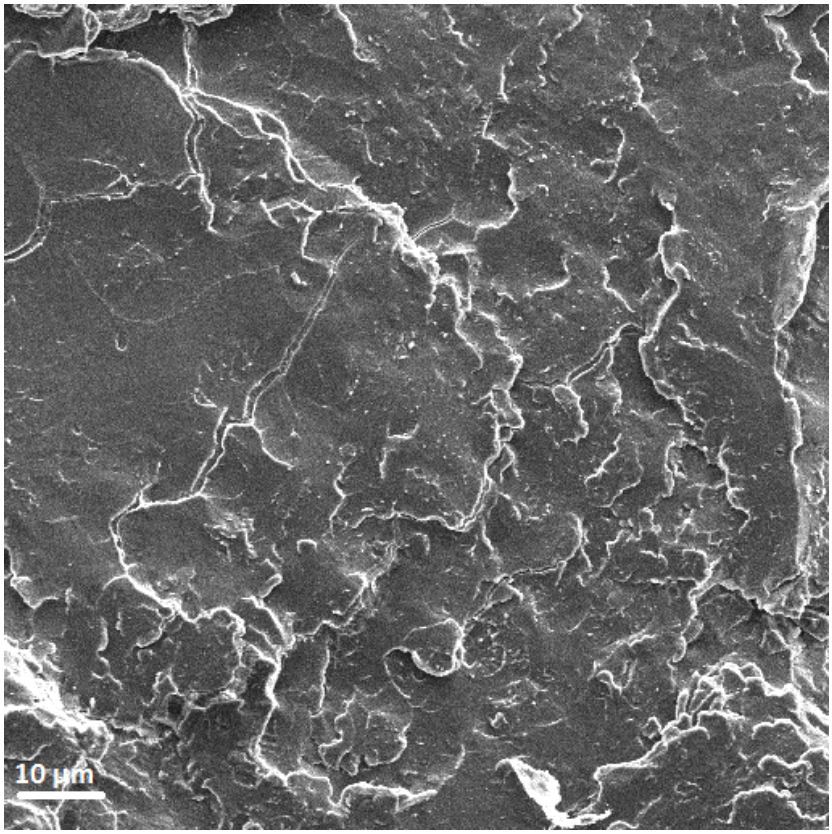

Figure 28: Carbon black 0.005% 12000s→Beam voltage: 5kV& Working distance: 6mm.

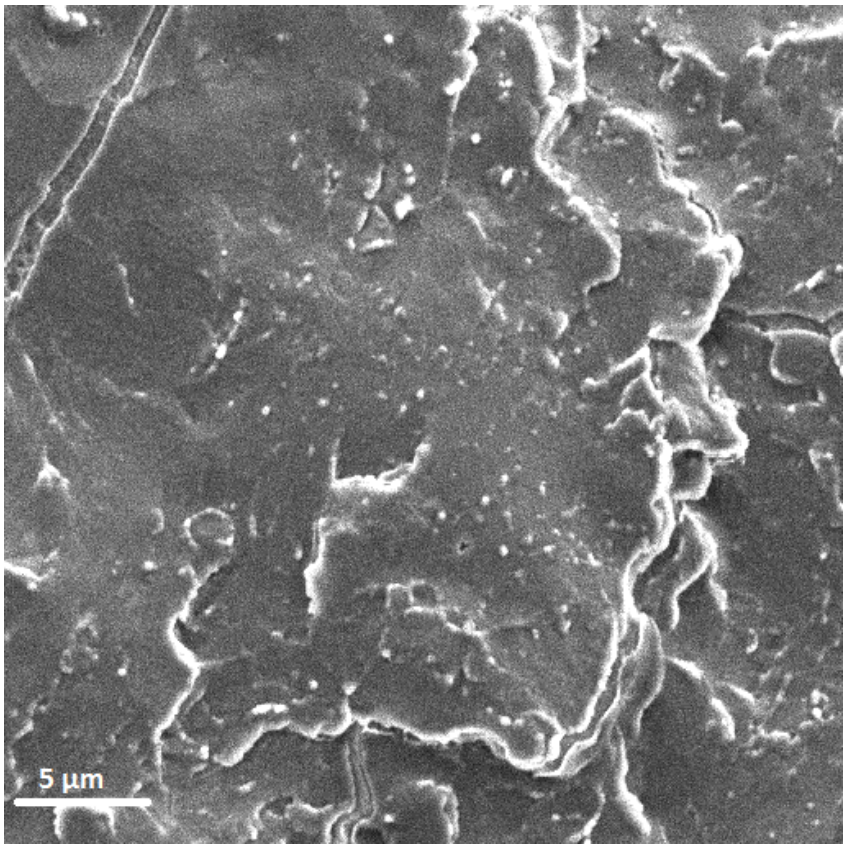

Figure 29: Carbon black 0.005% 12000s→Beam voltage: 5kV& Working distance: 6mm.

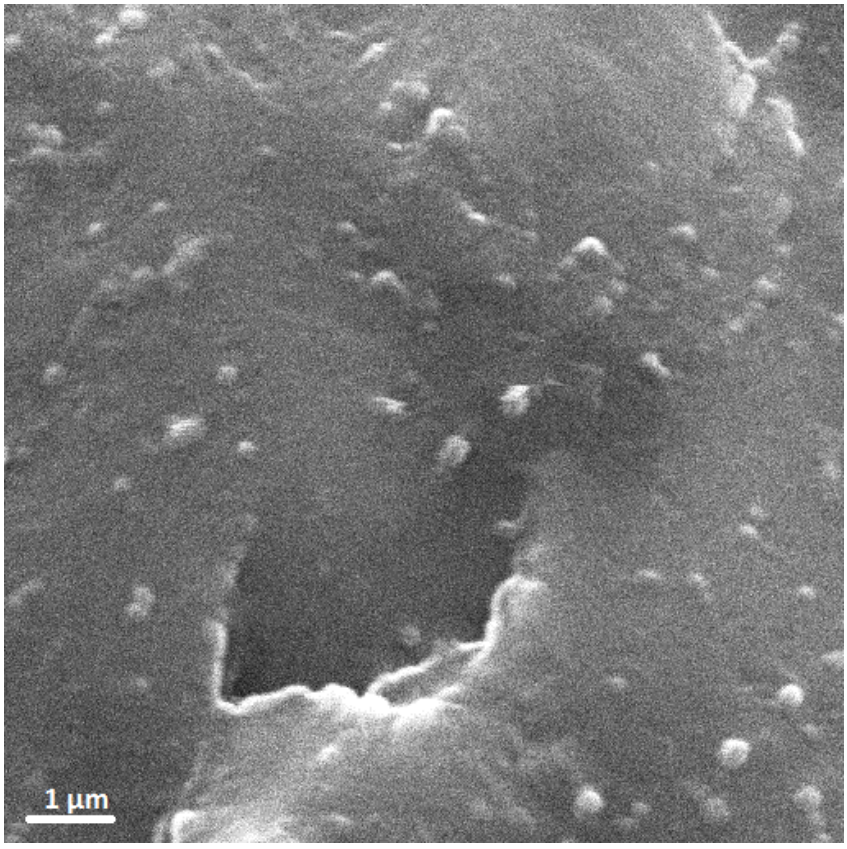

Figure 30: Carbon black 0.005% 12000s→Beam voltage: 10kV& Working distance: 6mm.